

Evaluating real-time particulate matter instruments against gravimetric and size-resolved references to advance residential wood heater development

Vi H. Rapp^{a,*}, Brett C. Singer^a, Rebecca Trojanowski^b, Sharon S. Chen^a, Dylan Anacleto-Black^a, William W. Delp^a, Eric Adair^c, John Crouch^c

^a*Energy Technologies Area, Lawrence Berkeley National Laboratory, Berkeley CA, United States*

^b*Interdisciplinary Science Department, Brookhaven National Laboratory, Upton NY, United States*

^c*Hearth, Patio and Barbecue Association, Arlington, VA, United States*

Abstract

Residential wood heater certification testing relies on time-integrated gravimetric filters that obscure the transient particulate matter (PM) generation events central to heater certification. Continuous PM instruments could support advancement of heater technologies, but most are developed for ambient air and may struggle under the high concentrations, dynamic transients, and variable aerosol properties of wood combustion. This study evaluated five continuous PM instruments spanning light scattering (TSI DustTrak II 8530, Thermo MIE pDR-1500, Particles Plus 8306), inertial mass (Thermo Scientific 1405-D TEOM), and triboelectric charge (Sintrol S203) against gravimetric filters and size-resolved reference concentrations across three heater types and two operating phases. No single instrument performed well across all conditions. The DustTrak II and pDR-1500 demonstrated the most consistent temporal tracking ($r \geq 0.87$ and $r \geq 0.79$, respectively) but substantially overestimated integrated PM mass during cordwood combustion and require gravimetric correction for quantitative use. The TEOM performed closest to the gravimetric reference during pellet high-burn phases but exhibited sustained negative cumulative mass during cordwood tests. The Particles Plus and Sintrol showed the weakest overall performance across all conditions. These results support the continued advancement of residential wood heater technologies by identifying conditions under which each instrument provides more or less reliable PM data, and may help inform instrument selection for laboratory testing for product development and field studies for verification.

Keywords: wood smoke aerosol, TEOM, optical particle counter, triboelectric monitor, biomass combustion, light-scattering photometer

*Corresponding author: vhapp@lbl.gov

1. Introduction

Globally, domestic biomass combustion continues to be an essential residential heating method. With tens of millions of households across the United States and Europe relying on wood for primary or secondary heating, successive generations of heater design have substantially reduced particulate matter (PM) generation over the past decade [10, 14, 32, 61, 65, 66]. As manufacturers refine heater designs and regulators develop certification frameworks that reflect real-world operation, continued advancement of residential wood heating technologies requires measurement tools capable of resolving the transient combustion events that may increase PM generation. Time-integrated gravimetric methods, which have served as the cornerstone of international certification testing for approximately four decades, do not provide this temporal resolution and instead average transient events into a single cumulative value [5–9, 16, 19, 23, 51, 56, 67].

To capture transient PM events, EPA ALT-140, an alternative certification test method, incorporates a continuous PM mass instrument during certification [67]. This method utilizes a Tapered Element Oscillating Microbalance (TEOM) to measure PM mass directly from the dilution tunnel at 1-minute intervals [67]. While the TEOM can log data at 10-second intervals, it is subject to signal noise that can reduce precision [57, 58]. Furthermore, the instrument is bulky, expensive, and faces operational challenges in combustion environments [2, 3, 18, 28, 30, 37, 52, 57]. For instance, its collection filters are prone to rapid overloading under heavy particulate loads, requiring multiple manual filter changes within a single test cycle [2, 31, 33, 57]. The heated sensor element can also trigger volatilization of semi-volatile compounds or experience mechanical shedding from filter oscillation under dynamic flows, leading to significant measurement fluctuations [3, 20, 37, 40, 50]. Although the instrument has proven viable for laboratory testing of wood heaters, studies using the TEOM with wood heaters in the field are limited [37, 52, 69]. Also, the manufacturer announced that production of the TEOM is ending, with no orders accepted after June 30, 2026.

Integrating portable, continuous PM measurements could enhance wood heater designs while expanding understanding of wood heater performance in the laboratory and the field. However, the vast majority of continuous PM instruments are designed for ambient conditions with low mass concentrations and stable, near-ambient temperatures [3, 57, 58]. Wood combustion exhaust, by contrast, presents a harsh, high-concentration environment (>400 mg/m³ when sampling from the dilution tunnel) that can challenge the operation and measurement range of many PM instruments.

Light-scattering instruments offer an appealing alternative to the TEOM due to their portability and ease of use [1, 30, 54]. Yet, their application to wood heater testing is complicated by aerosol morphology [1, 26, 44]. A substantial portion of the PM generated during wood combustion consists of particles smaller

33 than 300 nm in diameter [12, 13, 17, 24, 62]. Because many portable optical monitors have an effective lower
34 detection limit of about 100 – 300 nm, they can significantly underpredict total mass [1, 26, 44, 54, 69].
35 Factory-calibrated scaling algorithms can partially compensate, but they frequently fail to account for the
36 unique refractive indices of wood smoke and shifts in the sub-300 nm particle fraction across combustion
37 conditions [63]. Conversely, some monitors may overcompensate via these internal algorithms, leading to
38 overprediction during peak events [1, 44, 54]. While co-located gravimetric filters can be used to calibrate
39 these optical responses, performing continuous filter corrections adds a substantial operational burden during
40 in-home field studies [70, 71].

41 To avoid filter loading and dilution complexities associated with TEOMs and light-scattering instruments,
42 some PM monitors can track particles directly from the undiluted exhaust stack. For example, opacity
43 sensors use light extinction to handle high-concentration pathways through direct visual attenuation [47, 49,
44 60]. Some specialized devices are designed to monitor particulate output directly from the chimney, while
45 other industrial monitors offer rugged designs that could be adapted to wood heaters [47, 49]. However,
46 many industrial opacity sensors require long physical path lengths to maintain measurement sensitivity,
47 and they require empirical calibrations to correlate raw opacity data to true PM mass [48, 60]. Similarly,
48 triboelectric monitors offer a rugged, filterless option for direct stack monitoring [22, 41]. Yet, their sensitivity
49 to particle charge, exhaust velocity, and composition variations remains poorly characterized under transient
50 operational phases [22]. Consequently, while both opacity and triboelectric instruments allow for direct
51 exhaust measurements, these options may be better suited for tracking relative PM trends rather than
52 providing real-time PM mass concentrations across laboratory and field settings.

53 The purpose of this paper is to (1) assess if any real-time instrument(s) could replace the integrated
54 gravimetric filter as the basis for a certification mass measurement; (2) determine if any instrument(s) can
55 provide time-resolved information to support heater design and combustion research; and (3) explore the
56 implications of these laboratory findings for assessing in-home performance. To achieve these goals, we
57 evaluate five real-time PM instruments for measuring wood heater PM across three heater types and two
58 operational phases. The instruments span three measurement principles: light-scattering (DustTrak II 8530,
59 MIE pDR-1500, and Particles Plus 8306), inertial mass measurement (TEOM 1405-D), and triboelectric (Sin-
60 trol S203). Each instrument is evaluated during startup, high-burn, and low-burn phases of three residential
61 room heater types (non-catalytic cordwood, catalytic cordwood, and pellet), with performance benchmarked
62 against laboratory-grade gravimetric and size-resolved mass references. Integrated mass measured by each
63 instrument was compared with the gravimetric reference, while temporal tracking of the PM measurements
64 were compared with the size-resolved mass reference. By identifying which instruments reliably provide
65 integrated mass measurements and resolve transient PM events across heater types and operating phases,

66 this work supports the measurement infrastructure needed for continued advancement of residential wood
67 heater technology.

68 2. Methods

69 2.1. Experimental Setup

70 Exhaust from the heaters was captured and diluted using a dilution tunnel system compliant with ASTM
71 E2515-11 [4]. To minimize particle losses, PM was sampled using a seamless, stainless-steel bent probe nozzle
72 recommended by EPA Method 5, instead of a straight sampling probe [68]. Dilution tunnel flow rates
73 were verified using a standard Pitot tube, and set to approximately 14.15 m³/min (~500 SCFM) for cord-
74 wood heaters and 8.5 m³/min (~300 SCFM) for the pellet heater. Type T exposed-junction thermocouples
75 measured dilution tunnel, ambient, and gravimetric sampling train temperatures, and an Omega RH-USB
76 sensor measured dilution tunnel relative humidity. All instrument outputs were displayed and logged using
77 a custom Python-based program. A schematic of the dilution tunnel system is shown in Figure 1.

78 A secondary dilution system kept sample concentrations within optimal instrument ranges and prevented
79 fouling by blending controlled flows of dilution tunnel aerosol and ultra-zero grade air from a gas cylinder.
80 The ultra-zero air met the following specifications: O₂ 19.5–23.5%, water < 2 ppm, hydrocarbons < 0.1 ppm,
81 CO₂ < 0.5 ppm, and CO < 0.5 ppm. The effective dilution factor was tracked in real time by comparing
82 carbon dioxide (CO₂) measurements in the secondary dilution line (PP Systems SBA-5 nondispersive infrared
83 (NDIR)-CO₂ analyzer) to those in the dilution tunnel (California Analytical Instruments 600 Series NDIR
84 analyzer). Gas analyzers were zeroed and spanned at the start of each test day and zero-checked at the end
85 of each test day. Secondary dilution ranges for each phase are summarized in Table S1.

86 2.2. Heater Specifications

87 Experiments were conducted with three wood heaters: a catalytic cordwood heater (Blaze King Sirocco
88 SC20.2), a non-catalytic cordwood heater (Quadra-Fire 4300 Millennium), and a pellet heater (Regency
89 Greenfire GF55). The catalytic cordwood heater has a 1.8 cu. ft (0.051 cu. m) firebox and was acquired new
90 in 2023. The non-catalytic cordwood heater has a 2.3 cu. ft (0.065 cu. m) firebox and was obtained used
91 from the manufacturer following quality control testing in 2025. The pellet heater was purchased new in
92 2024. Prior to use in these experiments, each heater was pre-conditioned by undergoing at least 48-hours of
93 operation at medium-to-high burn rates. Each heater was installed with a chimney stack following standard
94 laboratory test methods [5–8]; details about the chimney materials and heights are provided in Section S-1.2.

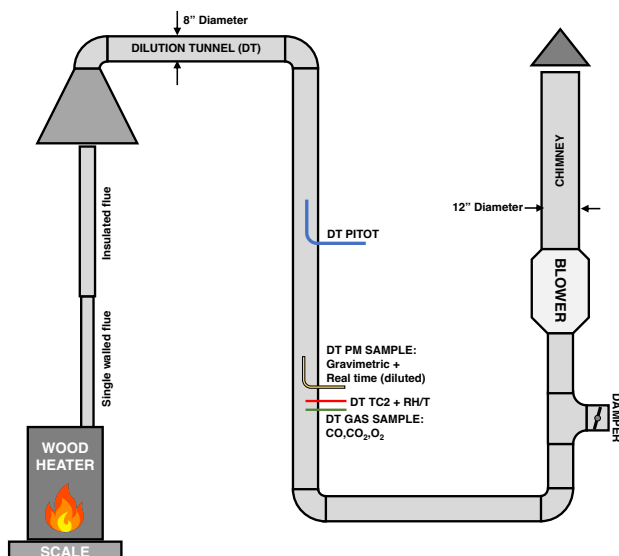


Figure 1: Schematic of laboratory experimental setup with dilution tunnel (DT). Note: TC is thermocouple, P is pressure, and PM is particulate matter.

95 2.2.1. Heater Operation

96 Each heater was operated in two phases: a *high-burn* phase, capturing cold (room-temperature) startup
 97 through steady-state operation at near-maximum burn rates, and a *low-burn* phase, capturing turndown
 98 through steady-state operation at near-minimum burn rates. Two replicate tests were conducted for each
 99 heater and phase, for a total of 12 tests. Initial conditions, heater settings, and key events for each phase
 100 are provided in Section S-1.3. Consistent with certification practice, burn phases are defined by the firebox
 101 initial conditions: a high-burn phase begins from a cold (room-temperature) firebox and a low-burn phase
 102 begins from a hot coal bed. Because each phase is established by these initial conditions, more than one
 103 phase may be conducted on a single test day.

104 The high-burn phase for the cordwood heaters begins with ignition of paper, kindling, and small logs in
 105 a cold firebox with air controls set to maximum (~10-20 minutes). A charge of two to five larger logs is
 106 added once the firebox is hot. For the catalytic cordwood heater, the catalyst is engaged immediately after
 107 loading this charge. The heater then operates at high output for the remainder of the phase. The pellet
 108 heater's high-burn phase includes an automated 10-15 minute startup sequence initiated when the heater is
 109 powered on. After startup, it operates at 'Heat Level 5' for the remainder of the phase.

110 The low-burn phase for the cordwood heaters begins with a fresh reload of 2-3 larger logs, after which

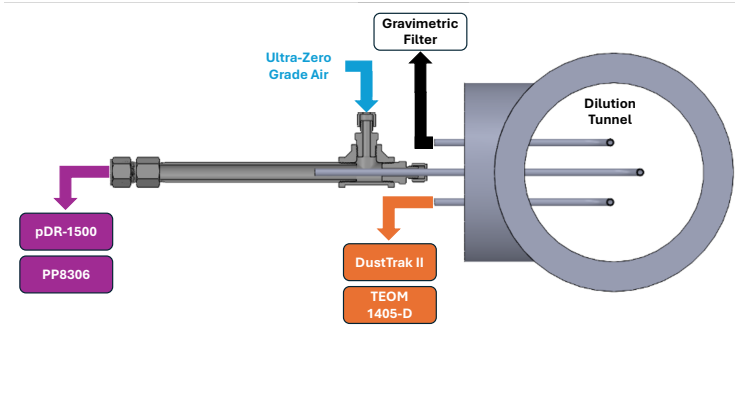


Figure 2: Cross-sectional schematic of 90° bent-sampling probes viewed from the bottom of the dilution tunnel, and the secondary dilution system to PM instruments.

111 the burn rate controls are reduced to their low-burn settings. The non-catalytic cordwood heater has an
 112 Automatic Combustion Control (ACC) in addition to a burn rate lever. The ACC provides additional
 113 combustion air that is automatically controlled over approximately 25 minutes to quickly ignite new logs.
 114 The manual recommends engaging the ACC right before adding fuel. It should be noted that during the
 115 second low-burn test, the ACC was engaged about 5-minutes after loading the fuel, which increased PM
 116 generation. Burn rate for the catalytic cordwood heater is reduced manually by stepping down the thermostat
 117 adjustment twice over the first 10 minutes. Each phase continues until less than 1.0 kg of fuel (based on
 118 the scale reading) remains in the firebox. The pellet heater’s low-burn phase begins when the operator
 119 selects Heat Level 2. The heater automatically reduces the pellet feed rate and operates at steady-state for
 120 approximately 2 hours, after which it is powered off. The final 10 minutes of the low-burn phase captures
 121 a portion of the heater’s automated shutdown sequence, in which all remaining pellets in the burn-pot are
 122 extinguished. This corresponds to the first 10 minutes of the 40-minute shutdown sequence outlined in the
 123 certification test.

124 All heaters were fueled with Douglas fir. Seasoned cordwood was sourced locally in 2023 and pellets
 125 purchased in 2020. The dry fuel consumption during each heater operating phase is reported in Table 1.
 126 Additional details about the fuel, including composition and moisture content, can be found in Section S-1.4.

Table 1: Dry fuel consumed in kilograms for each heater by test phase. Two replicate tests were conducted for each heater and each operating phase.

Phase	Test	Non-Cat Cordwood (kg)	Cat-Cordwood (kg)	Pellet (kg)
High-burn	1	7.1	3.3	2.1
	2	4.9	3.3	2.1
Low-burn	1	1.2	2.3	2.1
	2	1.3	2.8	2.0

127 *2.3. Reference Particle Methods*

128 To evaluate the accuracy and temporal response of the five PM instruments, their cumulative mass
129 and real-time measurements were compared against two references: a gravimetric filter measurement and
130 reconstructed mass concentration derived from three particle size spectrometers spanning 5.6 nm to 20 μm .

131 The reference cumulative PM mass for each phase was determined gravimetrically using a modified version
132 of test method ASTM E2515-11 [4]. Exhaust from the dilution tunnel was sampled iso-axially through a
133 filter train containing two pre-weighed 47 mm PTFE-bonded glass fiber filters (Cytiva Pallflex Emfab™)
134 mounted in series. A single gravimetric filter train was deployed per operational phase and filters were
135 replaced prior to each phase to ensure each integrated mass measurement corresponded to a single phase.
136 For the non-catalytic cordwood heater, all instrument sampling was stopped about 15 minutes after startup
137 to replace the reference filter and the DustTrak II filter. This was necessary to prevent filter overloading
138 and about 5-minutes of startup data was not recorded. After the filters were replaced, instrument sampling
139 resumed and the high-burn logs were added into the firebox. Flow rates across the filter train were held
140 constant at about 3 liters per minute (LPM) for all operating phases except for the second low-burn phase
141 of the non-catalytic cordwood heater, which was held constant 6 LPM. The flow rate for this phase was
142 increased to ensure filter masses would exceed the minimum accuracy of the microbalance.

143 The net catches from the two cordwood high-burn filter trains were summed to yield a single integrated
144 startup-plus-high reference mass, consistent with the single-filter treatment of the catalytic cordwood and
145 pellet high-burn phases. Pre- and post-test filter weights were measured on an ultramicrobalance. Cumula-
146 tive PM mass for each phase was calculated as the sum of net catches on both filters. Filter holders, gaskets,
147 and probes were flushed at the start and inspected at the end of each test day; PM deposition on these
148 surfaces was visually confirmed to be negligible and was not quantified.

149 The reference real-time mass concentration (hereon referred to as the size-resolved mass reference) was
150 reconstructed from three particle size spectrometers: a TSI 3321 Aerodynamic Particle Sizer (APS), TSI
151 3330 Optical Particle Sizer (OPS), and TSI 3091 Fast Mobility Particle Sizer (FMPS). Together, these
152 instruments measured particle number concentration from 6 nm to 20 μm at 1 Hz, spanning a size range no
153 single instrument covers. To prevent double-counting in regions of overlapping detection, bins at the edges
154 of each instrument's range were excluded. The FMPS contributed bins below 300 nm, the OPS bins from
155 300 to 700 nm, and the APS bins above 700 nm, with each boundary assigned to a single instrument. Time-
156 resolved particle counts were converted to mass concentration using per-phase effective densities derived from
157 the gravimetric filter measurements (see Section 2.5). All three instruments sampled from the secondary
158 dilution line (Figure 2) and were zeroed with Ultra-Zero grade air at the start of each test day. Further
159 details on the FMPS, OPS, and APS are provided in Section S-1.5.

160 *2.4. Particulate Instruments*

161 Five continuous PM instruments were evaluated across three residential wood heater types operating
162 in startup, high, and low-burn phases. Instruments evaluated included light-scattering (TSI DustTrak II
163 8530, Thermo Scientific MIE pDR-1500, and Particles Plus 8306), inertial mass measurement (Thermo
164 Scientific TEOM 1405-D), and triboelectric (Sintrol S203). Instruments were operated per the manufacturers
165 instructions with the exception of the TEOM. A brief summary of each instrument and how it was operated
166 is provided below. Additional details about each instrument can be found in Section S-2.6.

167 *DustTrak II 8530.* The TSI DustTrak II 8530 (DT2) is a single-channel, 90° light scattering, photometric
168 instrument that uses a laser diode to determine the mass concentration of aerosols in real time [63, 64]. Re-
169 lated models in this family include the EP version, which uses an external pump, and the DRX family, which
170 provides multi-channel mass fraction reporting. According to specifications, the DT2 has a concentration
171 range of 0.001 to 400 mg/m³ and detects particle sizes from 0.1 to 10 μm. The DT2 is calibrated against
172 a reference photometer that is gravimetrically calibrated to ISO 12103-1, A1 ultrafine test dust (Arizona
173 Test Dust). While the raw, A1 dust features a geometric median diameter of approximately 3 to 5 μm, the
174 size-selective aerosolization process utilized during factory calibration isolates a cloud with a mass median
175 aerodynamic particle diameter of 2.5 μm. The instrument software interprets this standard using a blended
176 material refractive index of 1.51 and assumes a solid particle density of 2.65 g/cm³ [63, 64]. The test dust
177 consists primarily of silicon dioxide and aluminum oxide, which together account for roughly 80% to 90% of
178 its total mass, supplemented by minor amounts of iron, alkali metals, and alkaline earth metals.

179 The DT2 features an internal 37 mm filter cassette for concurrent gravimetric sampling, which the
180 manufacturer recommends using to establish aerosol-specific photometric calibration factors. Of the total
181 3.0 LPM sample flow, two-thirds passes through the internal gravimetric filter as sample flow, with the
182 remaining one-third diverted as sheath flow. The internal flow controller maintains this total flow to within
183 ±5% of the factory set point [64]. The DT2 sampled directly from the dilution tunnel since past experience
184 demonstrated it could recover if concentrations exceeded its maximum limit. The 37 mm filter was replaced
185 at the beginning of each test phase to coincide with the replacement of the 47 mm reference filter, ensuring
186 identical sampling durations for a parallel comparison. Although particle size selection can be performed
187 using optional inlet impactors, no impactors were used in this study. On the morning of each test day, the
188 internal filter elements (sheath air HEPA filters) were replaced, and a zero calibration was performed using
189 an inline HEPA filter. The total flow rate was also confirmed at the beginning of each test day and monitored
190 after each filter change.

191 *MIE pDR-1500*. The Thermo Scientific MIE pDR-1500 (pDR) is a nephelometric monitor designed for
192 personal sampling that uses infrared scattering from an 880 nm Light Emitting Diode (LED) to estimate
193 PM mass concentrations [59]. According to its specifications, the pDR has a measurement range of 0.001 to
194 400 mg/m^3 and responds to an optical particle size range of approximately 0.1 to $10 \text{ }\mu\text{m}$. It is calibrated
195 against a reference monitor that is gravimetrically calibrated to ISO 12103-1, A2 Fine Arizona Test Dust
196 (historically SAE Fine). While the dry test dust possesses a geometric median diameter of approximately
197 $10 \text{ }\mu\text{m}$, the manufacturer notes that upon aerosolization into the instrument’s calibration chamber, the
198 floating fraction yields a mass median aerodynamic particle diameter of 2 to $3 \text{ }\mu\text{m}$ with a geometric standard
199 deviation of 2.5. The manual also references a calibration material refractive index of 1.54 (corresponding
200 to silicon dioxide) and defines the bulk density as 2.60 to 2.65 g/cm^3 [59].

201 Downstream of the photometric sensing stage, the monitor incorporates a 37 mm filter holder that protects
202 the pump from any sampled aerosol and serves as a sample collection filter for gravimetric analysis [59]. For
203 this study, the red inlet cyclone (Model GK 2.05) was used at a flow rate of 1.19 LPM, corresponding to
204 an approximate PM_{10} aerodynamic cut point [59]. The pDR sampled from the secondary dilution system
205 (Figure 2) to maintain concentrations within its operating range. At this dilution level, the mass collected on
206 the 37 mm filter fell within the weighing uncertainty of the microbalance, making a meaningful gravimetric
207 comparison with the 47 mm reference filter unreliable. On the morning of each test day, a zero calibration
208 was completed using an inline HEPA filter. The relative humidity correction was disabled and the calibration
209 factor was set to 1.000.

210 *Particles Plus 8306*. The Particles Plus 8306 (PP8306) is an optical particle counter designed to measure
211 real-time particle counts and approximate total mass concentrations from light-scattering data [45]. The
212 handheld instrument utilizes laser diode technology to sample air at a volumetric flow rate of 2.83 LPM
213 controlled by an internal vacuum pump. Operating across a concentration range of 0.01 to $20,000 \text{ }\mu\text{g/m}^3$,
214 the PP8306 sorts detected particles into six size channels ranging from 0.3 to $10.0 \text{ }\mu\text{m}$. To translate these
215 raw optical counts into real-time mass concentrations ($\mu\text{g/m}^3$), the internal firmware calculates the weight
216 of the sample using the average size of each channel alongside user-defined density and refractive index
217 adjustments. The PP8306 complies with ISO 21501-4 and JIS B9921 standards, and is calibrated using a
218 National Institute of Standards and Technology (NIST) traceable source, typically polystyrene spheres, at
219 specific particle size channels: 0.3, 0.5, 1.0, 2.5, 5.0, and $10.0 \text{ }\mu\text{m}$ [29]. The polystyrene spheres typically
220 have an average particle density of 1.05 g/cm^3 and a refractive index of 1.59.

221 The PP8306 sampled from the secondary dilution system to prevent concentrations from exceeding its
222 operating range. For this study, the mass density for each channel was set to 1.26 g/mL based on previous

223 experiments using Douglas fir and validated with experimental data collected in this study [46]. The refractive
224 index was set to 1.56 matching previous research measuring properties for Douglas fir smoke aerosol [27, 36].
225 To be consistent with the other instruments, the total PM mass concentration is reported in this study. At
226 the beginning of each test day, a zero-count check was conducted using an inline HEPA filter.

227 *Thermo Scientific TEOM 1405-D*. The Thermo Scientific TEOM 1405-D is a dual-channel real-time mass
228 monitor that incorporates two independent tapered element oscillating microbalance systems within a single
229 instrument chassis [58]. Because EPA references two different standard operating procedures for using the
230 TEOM with wood heaters, we followed the newest protocols with minor deviations [43, 67]. Specifically,
231 the impactor was removed for this study so both channels provide the same PM_{Total} measurement, even
232 though the system is designed as a dichotomous monitor to simultaneously isolate and measure $PM_{2.5}$ and
233 PM_{Coarse} fractions using a virtual impactor. This modification allows for side-by-side monitoring to verify
234 data consistency. The internal sample stream heaters were also disconnected [43].

235 The TEOM sampled directly from the dilution tunnel. Instrument setup, routine operations, and filter
236 handling procedures generally followed the standard operating procedure recommended by EPA [43]. At the
237 beginning of each test day, the TEOM internal clock and data logging configurations were verified. New,
238 Pallflex TX40 filter cartridges, were installed with a nominal sample flow rate set to 1.00 LPM for the
239 pellet and catalytic-cordwood heaters and 0.50 LPM for the non-catalytic cordwood heater to prevent filter
240 overloading. The instrument was operated for at least 1 hour, sampling clean air from a flowing dilution
241 tunnel, to allow pressure-related pneumatic transients to fully stabilize. Leak and flow checks were conducted
242 on both channels before installing new filters and immediately following test completion using a certified
243 reference flow meter. Pre-test criteria mandated a leak rate of ≤ 0.10 LPM and flow rate within 2.0% of the
244 setpoint (1.00 LPM), whereas post-test limits were set to ≤ 0.15 LPM for leaks and within 4.0% for flow. A
245 single filter set was used for each test where possible, with replacement occurring before filter loading reached
246 100% to ensure valid instrument operation and maintain sample flow control [43]. When a filter change was
247 required, the filters on both channels were replaced simultaneously and system stability was verified before
248 resuming collection.

249 Deviating from the 60-second reporting protocols outlined in the EPA-recommended standard operating
250 procedures, the TEOM data were recorded at 10-second intervals to fully characterize transient operational
251 phases, such as heater startup [43]. At 10-second resolution, each measurement reflects the mass accumulated
252 over a shorter interval, resulting in a lower signal-to-noise ratio and potentially a reduced per-point precision
253 compared to 60-second measurements; however, the cumulative mass and therefore the mean concentration
254 over the same sampling period should be equally accurate [34, 42]. Higher time-resolution data also revealed

255 localized instrument transients such as particle shedding and instantaneous negative mass concentrations
 256 that have been observed in previous research [3, 20, 37, 40, 50, 57]. Retaining the negative concentration
 257 values was necessary to prevent artificial inflation of the cumulative mass calculation [37]; the older EPA
 258 operating procedures also recommend retaining negative measurements [67].

259 *Sintrol S203 Dust Monitor.* The Sintrol S203 (Sintrol) is an in-duct dust monitor designed for continuous
 260 measurement of total suspended particles (TSP) in industrial process airflows [55]. The instrument oper-
 261 ates on the principle of inductive electrification, in which an isolated stainless-steel sensor probe is inserted
 262 perpendicular to the airflow; as charged particles pass near the probe, they induce an AC signal that is
 263 proportional to dust concentration. According to the manufacturer, the instrument has a detection limit of
 264 0.01 mg/m^3 and responds optimally to particles between 1 and $200 \text{ }\mu\text{m}$. Unlike the photometric instruments
 265 described above, converting the inductive signal to a mass concentration requires a material-specific cali-
 266 bration factor that accounts for differences in particle charge generation across dust types, sizes, and flow
 267 conditions [22]. The manufacturer states that the signal response is linear up to several hundred mg per
 268 cubic meter, beyond which it becomes nonlinear before reaching saturation at several grams per cubic me-
 269 ter [55]. The specifications also note that it has a minimum detectable particle size of $0.3 \text{ }\mu\text{m}$ and a minimum
 270 recommended duct flow velocity of 3 m/s . Because the S203 does not support entry of a material-specific
 271 calibration factor, data were logged in Inductive Electrification Units (IEU) and converted to mass concen-
 272 tration in post-processing using the 47 mm gravimetric reference measurements. The Sintrol was installed
 273 in the horizontal section of the dilution tunnel after the other PM instruments, located approximately five
 274 duct-diameters from the upstream elbow and three duct-diameters from the downstream elbow (see Figure
 275 1). The probe extended approximately 6.75 inches (190 mm) into the 8-inch (203 mm) diameter duct and
 276 logged data at a 50-second signal averaging interval. At the beginning of each test day, the Sintrol probe was
 277 cleaned, proper grounding was confirmed per the manufacturer’s instructions, and baseline measurements
 278 were collected with the dilution tunnel sampling ambient air [55].

279 2.5. Data Analysis for Size-Resolved Mass Reference

280 To calculate the size-resolved mass concentration reference at each time step, $M_{\text{ref}}(t)$, an effective particle
 281 density was determined for each phase using an iterative algorithm that reconciled particle size distribution
 282 measurements from the FMPS, OPS, and APS with gravimetric filter measurements. The algorithm started
 283 by assuming a density of 1.0 g/cm^3 and then converted the FMPS mobility diameters to aerodynamic
 284 diameter using

$$d_a = d_m \sqrt{\rho_e / \rho_0} \quad (1)$$

285 where d_a is aerodynamic diameter, d_m is mobility diameter, ρ_e is the effective particle density, and ρ_0 is a
 286 unit density (1.0 g/cm^3).

287 Next, the total particle volume across all particle instruments was calculated for a sampling time that
 288 matched the gravimetric measurement sampling time. This was done by calculating the total particle number
 289 distribution over the course of the test for each particle bin using,

$$N_{\text{test}}[\#] = \sum_{d=d_i}^{d=d_f} \sum_{t=0}^{t_{\text{test}}} \left(\frac{dN}{d \log D_p} \right)_d \left[\frac{\#}{\text{cm}^3} \right] \cdot \bar{Q}_{\text{duct}} \left[\frac{\text{m}^3}{\text{s}} \right] \cdot \Delta t [\text{s}] \cdot d \log D_p \cdot \frac{10^6 \text{ cm}^3}{1 \text{ m}^3} \quad (2)$$

290 where t_{test} is the duration of the test in seconds, \bar{Q}_{duct} is the mean dilution tunnel volumetric flow rate, and
 291 Δt is the sampling interval, equal to 1 second for all instruments. Then, the total particle volume during
 292 the sampling period was calculated using,

$$V_{\text{test}} [\text{cm}^3] = \frac{1}{6} \pi d^3 [\text{nm}^3] \cdot N_{\text{test}}[\#] \cdot \frac{10^{-21} \text{ cm}^3}{1 \text{ nm}^3}, \quad (3)$$

293 and the effective density was calculated using,

$$\rho_e \left[\frac{\text{g}}{\text{cm}^3} \right] = \frac{M_{\text{filt}} [\text{mg}]}{V_{\text{test}} [\text{cm}^3] \cdot \frac{1000 \text{ mg}}{1 \text{ g}}}, \quad (4)$$

294 where M_{filt} is the total gravimetric mass collected on the filter over the test duration, and V_{test} is the
 295 integrated particle volume computed from the three spectrometers.

296 The calculated ρ_e was compared with the initial guess; if the values differed by more than 0.1%, the
 297 updated ρ_e (Equation 4) was used to convert the FMPS mobility diameters to aerodynamic diameters
 298 (Equation 1) and the cycle was repeated. Damping (weighted averaging with the previous iteration using
 299 $\alpha = 0.5$) and safeguards to detect physically unrealistic density values (≤ 0 or $> 20 \text{ g/cm}^3$) were applied to
 300 stabilize convergence, with a maximum iteration limit of 1000. The resulting per-phase effective densities
 301 are reported in Table S9.

302 With the effective density converged and the FMPS bin diameters corrected, the total particle number,
 303 $dN(t)$, over a specified diameter range was calculated at each time step using,

$$dN(t) \left[\frac{\#}{\text{m}^3} \right] = \sum_{d=d_i}^{d=d_f} \left(\frac{dN(t)}{d \log D_p} \right)_d \left[\frac{\#}{\text{cm}^3} \right] \cdot d \log(D_p) \cdot \frac{10^6 \text{ cm}^3}{1 \text{ m}^3} \quad (5)$$

304 where $\frac{dN(t)}{d \log D_p}$ is the particle number concentration at time t for geometric mean diameter d , d_f and d_i
 305 are the upper and lower bounds of the particle diameter range in nm, and $d \log(D_p)$ is the log (base 10) of

306 the instrument-specific constant bin width. Note that units for each variable are presented in the square
307 brackets.

308 Next, the total particle volume, $dV(t)$, at a given time was calculated using

$$dV(t) \left[\frac{\text{cm}^3}{\text{m}^3} \right] = \frac{1}{6} \pi d^3 [\text{nm}^3] \cdot dN(t) \left[\frac{\#}{\text{m}^3} \right] \cdot \frac{10^{-21} \text{ cm}^3}{1 \text{ nm}^3} \quad (6)$$

309 Then, the total mass concentration, $dM(t)$, at a given time was calculated using

$$dM(t) \left[\frac{\text{mg}}{\text{m}^3} \right] = dV(t) \left[\frac{\text{cm}^3}{\text{m}^3} \right] \cdot \rho_e \left[\frac{\text{g}}{\text{cm}^3} \right] \cdot \frac{1000 \text{ mg}}{1 \text{ g}} \quad (7)$$

310 To avoid double-counting in the overlapping size ranges of the three spectrometers, the size-resolved mass
311 reference at each timestep was computed as the sum of $dM(t)$ from each instrument over its assigned,
312 non-overlapping diameter range (as described in Section 2.3):

$$M_{\text{ref}}(t) = dM_{\text{FMPS}}(t) + dM_{\text{OPS}}(t) + dM_{\text{APS}}(t), \quad (8)$$

313 where each instrument's contribution is evaluated over its assigned bin range.

314 2.6. Gravimetric Correction

315 For temporal concentration comparisons, all instruments were corrected to the 47 mm gravimetric ref-
316 erence measurement for each operational phase [35, 59, 64]. For each phase, the instrument concentration
317 data were time-averaged over the phase duration, accounting for the secondary dilution factor where ap-
318 plicable. This phase-averaged concentration was then compared to the time-integrated mass concentration
319 derived from the 47 mm gravimetric filter to yield a bulk correction factor. Each discrete data point in the
320 continuous time series was multiplied by this correction factor to produce the final gravimetrically corrected
321 PM mass concentration time series. For the Sintrol, the ambient baseline IEU signal was subtracted from
322 the raw measurements prior to applying the gravimetric correction. The correction factors derived for each
323 instrument and operational phase are reported in Table S8.

324 2.7. Statistical Analysis

325 Agreement between each PM instrument and the size-resolved reference mass concentration was assessed
326 using the Pearson correlation coefficient (r), which quantifies the strength and direction of the linear re-
327 lationship between two variables. The coefficient was calculated between each instrument's time-resolved
328 output and the reference mass concentration for each heater and operating phase. The Pearson r was se-
329 lected over the coefficient of determination (R^2) because its sign carries physically meaningful information,

330 as several instruments returned negative r values during low-burn and pellet phases, indicating an inverse
 331 relationship with the reference that would be obscured by squaring. Bland-Altman analysis and parity plots
 332 are also provided in the supplemental data to further evaluate systematic bias (median difference) and limits
 333 of agreement [11, 25, 38, 39, 53]. Because the data was not normally distributed, limits of agreement were
 334 calculated as the 2.5th and 97.5th percentiles rather than the mean $\pm 1.96 \times \text{SD}$. All metrics were computed
 335 on 10-second averaged data over each operating phase. Prior to all comparative analyses, continuous instru-
 336 ment time series were individually aligned to the size-resolved mass reference to correct for sampling-line
 337 and instrument response delays. For each instrument, the time offset relative to the size-resolved reference
 338 was estimated by finding the shift that gave the closest alignment between the two mass concentration time
 339 series during the high-burn phase. The same offset was then applied across all test phases for that instru-
 340 ment. A time offset was not applied to the Sintrol because its collection frequency was 50-seconds and the
 341 triboelectric output was not directly comparable to a mass concentration reference.

342 3. Results and Discussion

343 Five continuous PM instruments were evaluated against gravimetric filter and size-resolved reference
 344 concentrations across three heater types and two operating phases. Each instrument is assessed in terms of
 345 its agreement with the gravimetric reference measurement, its ability to capture transient PM events, and
 346 the practical implications of these findings for field deployment.

347 3.1. Gravimetric Reference Agreement

348 Table 2 reports the corresponding time-integrated PM mass from each instrument alongside the reference
 349 gravimetric filter and the DT2 onboard gravimetric filter. Figure 3 shows the mass ratio of each instrument
 350 to the gravimetric filter reference for each heater type and operating phase, where ratios greater than 1.0
 351 indicate overestimation (orange) and ratios less than 1.0 indicate underestimation (purple). Phases where
 352 the instrument reported a negative cumulative mass are excluded from the ratio comparison. No correction
 353 factors are applied to the real-time instrument data, and secondary dilution is accounted for where applicable
 354 (see Section 2.1). The Sintrol is excluded from this comparison because its triboelectric TSP output could
 355 not be converted to a total PM mass without using the gravimetric filter measurement.

356 *DT2 Gravimetric Filter.* The onboard gravimetric filter of the DT2 (DT2 Grav) showed generally good
 357 agreement with the reference across all heater types and phases, with mass ratios ranging from 0.63 to 1.00,
 358 consistently falling at or below unity. The closest agreement occurred during pellet heater operation, with
 359 ratios between 0.84 and 1.00 and no clear difference between high- and low-burn phases. Both cordwood

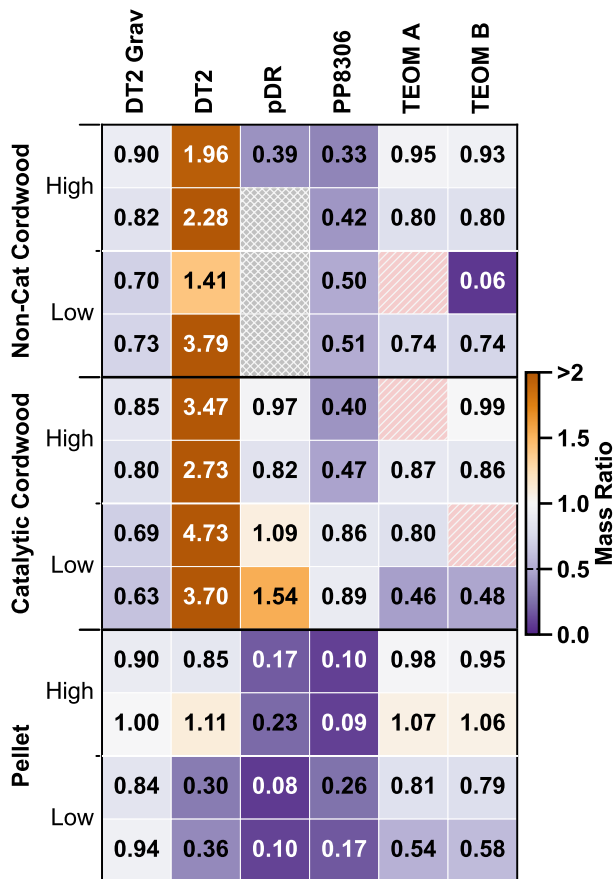


Figure 3: Mass ratio of each real-time instrument to the gravimetric filter reference for each heater type and operating phase. Ratios greater than 1.0 indicate overestimation (orange) relative to the reference, while ratios less than 1.0 indicate underestimation (purple). Hatched cells indicate phases where the instrument reported a negative cumulative mass. pDR data was not collected for three of the non-catalytic cordwood tests due to user error. The TEOM channel A reported negative mass for two cordwood tests while channel B reported negative mass for one cordwood test.

Table 2: Integrated PM mass from the gravimetric filter reference, the DustTrak II gravimetric filter (DT2 Grav), and time-integrated PM from the DustTrak II (DT2), pDR1500 (pDR), Particles Plus 8306 (PP8306), and both channels of the TEOM across all heater types and operating phases. All reported masses are in grams. pDR data was not collected for three of the non-catalytic cordwood tests due to user error. Note that the automatic air control for the second low-burn test for the non-catalytic cordwood heater was engaged late, leading to higher particulate matter generation than the first test.

Heater	Phase	Reference	DT2 Grav	DT2	pDR	PP8306	TEOM A	TEOM B
Non-Catalytic Cordwood	High 1	6.00	5.43	11.77	2.34	1.98	5.72	5.60
	High 2	6.96	5.68	15.87	—	2.89	5.58	5.60
	Low 1	0.72	0.50	1.01	—	0.36	-0.05	0.05
	Low 2	6.71	4.88	25.45	—	3.40	4.98	4.94
Catalytic Cordwood	High 1	9.87	8.37	34.31	9.56	3.99	-9.49	9.80
	High 2	6.48	5.19	17.68	5.30	3.05	5.61	5.56
	Low 1	1.08	0.74	5.09	1.17	0.93	0.87	-16.81
	Low 2	1.66	1.04	6.15	2.56	1.49	0.76	0.80
Pellet	High 1	2.06	1.85	1.76	0.36	0.20	2.01	1.96
	High 2	1.88	1.88	2.10	0.44	0.16	2.02	2.01
	Low 1	1.22	1.02	0.36	0.09	0.32	0.99	0.97
	Low 2	1.04	0.98	0.37	0.10	0.18	0.57	0.61

360 heaters showed substantially lower ratios during low-burn (0.63–0.73) compared to high-burn (0.80–0.90),
 361 and their high-burn ratios were on average lower than those observed for the pellet heater.

362 Several possible explanations for the DT2’s underestimation were considered. The ratio pattern across
 363 burn phases and heater types suggests that aerosol composition may be contributing to the DT2’s underesti-
 364 mation. Researchers have shown that PM from pellet combustion is predominantly solid inorganic material,
 365 consisting mainly of potassium and sulfate salts, while PM from cordwood combustion is dominated by
 366 organic matter and elemental carbon [15, 17, 24]. The lower ratios observed for heaters producing primarily
 367 organic PM suggest that evaporative loss of semi-volatile organics due to filter heating within the DT2 may
 368 be a contributing factor. Specifically, we hypothesize that internal temperatures within the DT2 enclosure
 369 may have increased over the course of a sampling day, resulting in elevated filter temperatures and greater
 370 evaporative losses during low-burn phases, which were always conducted later in the day. Although filter
 371 temperature inside the DT2 cassette was not monitored, post-test investigation revealed that temperatures
 372 near the DT2 filter cassette were consistently elevated above the reference filter and ambient. The cassette
 373 temperature continued to rise over the first hour of pump operation, with peak temperatures coinciding with
 374 the period in which low-burn sampling would typically begin (see Figure S8). While internal heating of the
 375 DT2 enclosure represents a source of negative bias, this is a known and tolerable limitation of in-situ optical
 376 measurements, where the ability to deploy a compact, battery-powered instrument in the field outweighs the
 377 cost of a modest systematic underestimation. This thermal bias may be partially reduced by using the DT2
 378 with an external pump; however, temperatures within the enclosure were observed to increase even with

379 the internal pump off, suggesting that pump heat is not the sole contributor to filter heating and that an
380 external pump configuration may only partially mitigate this effect (see Figure S8).

381 *Real-Time Instruments.* The performance of each real-time instrument varied widely across heater types
382 and operating phases, with no single instrument performing consistently well.

383 The DT2 exhibited a distinct pattern of overestimation for both cordwood heaters and near-unity agree-
384 ment for the pellet heater during high-burn, followed by severe underestimation during pellet low-burn.
385 Several potential explanations were considered. The calibration aerosol density (2.6 g/cm^3) substantially
386 exceeds the effective density of wood smoke aerosol (approximately $1.1\text{--}1.6 \text{ g/cm}^3$ depending on fuel type),
387 which would be expected to produce overestimation by approximately a factor of two if all else were equal.
388 This is broadly consistent with the overestimation observed for both cordwood heaters. The refractive in-
389 dex assumed during calibration (1.51) is slightly lower than that reported for wood smoke (1.56), which
390 would tend to cause underestimation, but not sufficient to offset the density-driven overestimation. For
391 the pellet heater, about 25–30% of total PM mass (see Figure S9) falls below the DT2’s stated detection
392 limit of $0.1 \text{ }\mu\text{m}$, which would contribute to underestimation. This may also partially explain the near-unity
393 agreement during pellet high-burn and reflect a coincidental cancellation of competing biases. The severe
394 underestimation during pellet low-burn (ratios of 0.30–0.36) may reflect the particle size distribution of the
395 aerosol. Low-burn combustion produces a lower fraction of particles larger than 300 nm , which generate a
396 disproportionately high optical response per unit mass. With fewer of these large particles present, the DT2
397 signal is suppressed relative to the true gravimetric mass, resulting in significant underprediction [44, 54].

398 The pDR performed closest to the reference during the catalytic cordwood phases, with ratios ranging
399 from 0.82 to 1.54, which may partly reflect the greater proportion of particles in the $300 \text{ nm}\text{--}1 \text{ }\mu\text{m}$ range
400 relative to non-catalytic cordwood combustion (see Figure S9, Test 1). Particles in this size range scatter
401 light more efficiently per unit mass than the sub- 300 nm particles that dominate non-catalytic exhaust[44],
402 potentially producing a stronger pDR response relative to collected mass. For the non-catalytic cordwood
403 heater, the pDR underestimated total PM mass during the high-burn (mass ratio of 0.39), but it is unclear
404 if this is representative for all non-catalytic cordwood heater tests since data from three of the four phases
405 were lost due to a pressure disturbance caused by user error. Severe underestimation was observed during
406 pellet heater operation, with ratios ranging from 0.08 to 0.23, consistent with the dominance of sub- 100 nm
407 particles in pellet smoke, which contribute little scattered signal relative to their mass. Although the pDR
408 and DT2 share the same stated lower detection limit of $0.1 \text{ }\mu\text{m}$, the two instruments show opposite biases
409 for cordwood aerosol, with the pDR underestimating and the DT2 overestimating relative to the gravimetric
410 reference. This divergence likely reflects differences in size-dependent scattering response arising from the

411 use of different calibration dust grades, specifically A2 fine for the pDR and A1 ultrafine for the DT2, which
412 may be related to the wavelengths of their light sources, though a full explanation would require detailed
413 characterization of each instrument’s response across the relevant particle size range.

414 The PP8306 underestimated PM mass across all conditions, with ratios ranging from 0.33 to 0.89 for the
415 cordwood heaters and 0.09 to 0.26 for the pellet heater. For both cordwood heaters, ratios were consistently
416 higher during low-burn than high-burn phases, with the catalytic cordwood low-burn producing the highest
417 ratios overall (0.86 and 0.89). The near-unity ratios observed during catalytic cordwood low-burn phases are
418 more difficult to interpret. Although 60% of catalytic cordwood PM mass falls below the PP8306’s 300 nm
419 detection threshold, suggesting substantial underestimation should persist, these conditions also produced
420 a proportionally larger coarse fraction (10–20 μm), which the PP8306 can detect and which may partially
421 offset the sub-300 nm deficit (Figure S9). This coarse-fraction effect may explain why ratios approach
422 unity under these specific conditions, though this interpretation remains tentative. During non-catalytic
423 cordwood operating phases, ratios ranged from 0.33 to 0.51, reflecting significant underestimation driven by
424 the sub-300 nm particle fraction. The most severe underestimation occurred during pellet heater operation,
425 consistent with the dominance of sub-300 nm particles in pellet smoke falling below the PP8306’s optical
426 detection threshold. Unlike the DT2 and pDR, the PP8306 lacks an onboard gravimetric filter for site-specific
427 calibration, relying instead on user-provided density and refractive index values to convert particle counts
428 to mass concentration. Even with aerosol-specific optical properties derived from concurrent size-resolved
429 measurements, the instrument substantially underestimated PM mass across most conditions, suggesting
430 its mass conversion approach has fundamental limitations for wood smoke aerosol that cannot be resolved
431 through optical property inputs alone.

432 The TEOM reported integrated mass concentrations that were closest to the reference filter, but reported
433 non-quantitative results for 2 of the 16 tests for Channel A and 3 of the 16 tests for Channel B. For all but
434 one test, at least one channel provided valid measurements when the other channel reported erroneous re-
435 sults. The TEOM performed especially well during pellet heater high-burn phases where both channels
436 produced ratios close to unity (TEOMA: 0.98 and 1.07; TEOMB: 0.95 and 1.06). This closer agreement
437 is expected given that the TEOM measures mass directly by monitoring changes in the resonant frequency
438 of a tapered element and is therefore not subject to the optical size threshold that limits the three optical
439 instruments. Performance degraded during cordwood combustion, where semi-volatile losses become more
440 influential relative to the total mass accumulated on the tapered element. Three phases produced anomalous
441 negative cumulative mass values (Table 2), a known artifact of the tapered-element measurement principle
442 arising from semi-volatile absorption and desorption or mechanical shedding [3, 20, 37, 40, 50], and are
443 excluded from the mass ratio comparison. The near-zero TEOMB ratio during the first non-catalytic cord-

444 wood low-burn (0.06) likely reflects near-detection-limit conditions rather than a true instrument bias, as
 445 the reference mass for that phase was exceptionally low (see Table 2). When both channels reported values,
 446 they generally produced similar ratios to one another; however, ratios remained variable and generally below
 447 unity, consistent with known tapered-element measurement artifacts during cordwood combustion.

448 *3.2. Response to Transient PM Events*

449 To evaluate each instrument’s ability to capture transient PM events, time-resolved PM mass concentra-
 450 tions from each instrument were compared against the size-resolved mass reference measurements across all
 451 heater types and operating phases. Figures 4 and 5 show the high-burn and low-burn phases, respectively.
 452 Data are shown as 10-second averages to align the sampling rates of the optical instruments with those of
 453 the TEOM. Figure 6 summarizes the Pearson correlation coefficient (r) between each instrument and the
 454 reference for each test and phase, providing a quantitative complement to the temporal traces. Parity plots
 455 and Bland–Altman plots for each instrument are also provided in the Supplementary Data (SD) (Section S-
 456 2.7). Reported concentrations for all instruments reflect gravimetric correction as described in Section 2.6
 457 and gravimetric correction factors are shown in Table S8.

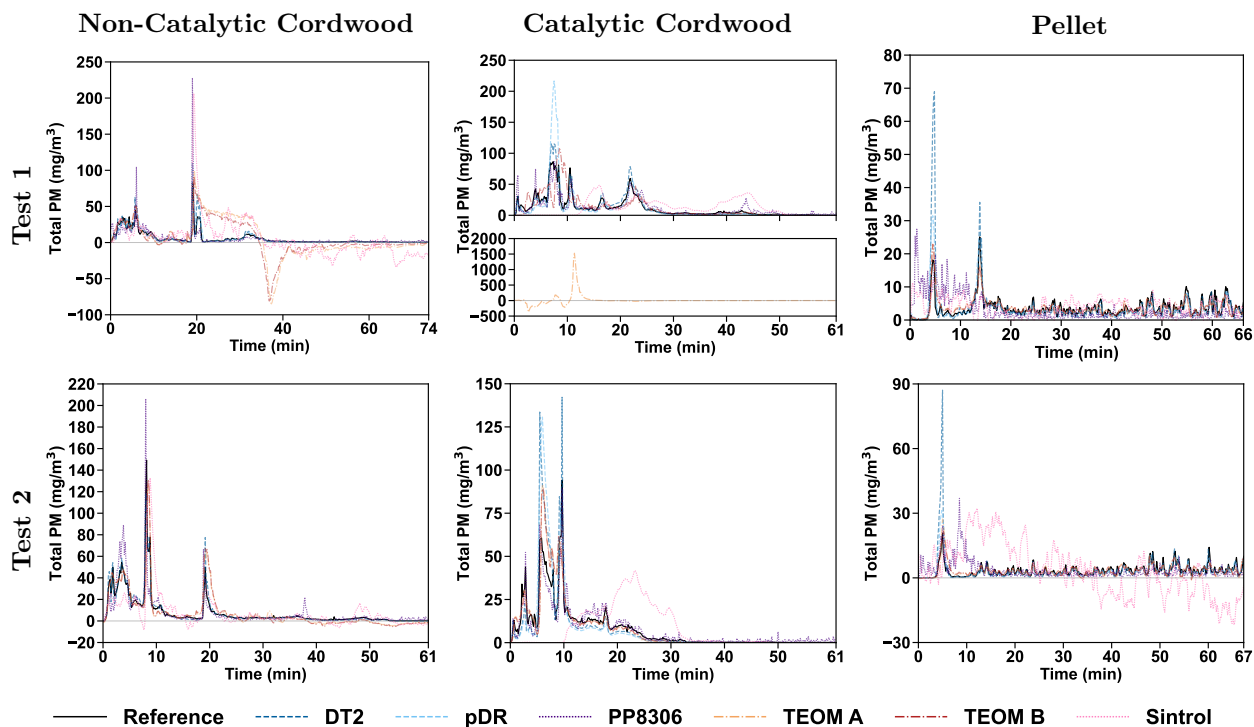


Figure 4: PM mass during high-burn phase for three heater types (columns) and two replicate tests (rows). The black solid line is the size-resolved mass reference. All instruments are gravimetrically corrected. TEOM A is only shown in the bottom for the catalytic cordwood Test 1 due to its large concentration range.

458 The DT2 and pDR consistently follow the general shape of the reference signal across all heater types and

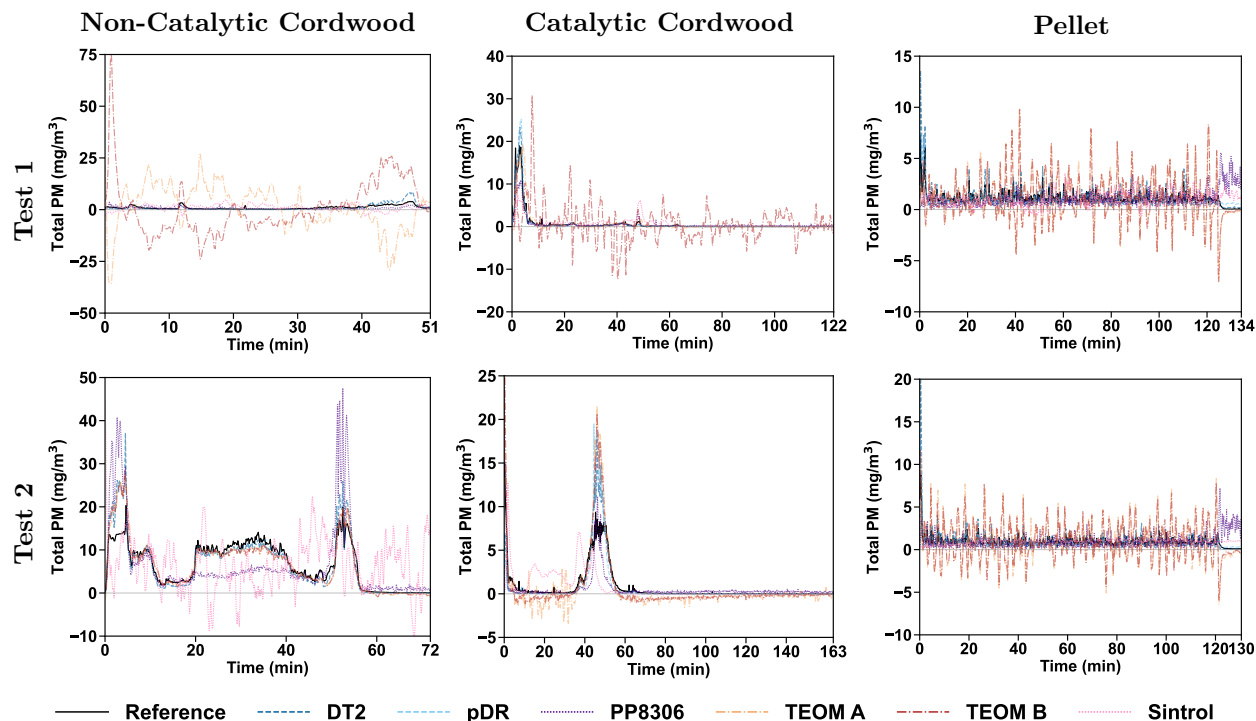


Figure 5: PM mass during low-burn phase for three heater types (columns) and two replicate tests (rows). All instruments are gravimetrically corrected. The black solid line is the size-resolved mass reference. Note that the automatic air control for the second low-burn test for the non-catalytic cordwood heater was engaged late, leading to higher particulate matter generation than the first test.

459 phases, capturing the emission events but not always the magnitudes. This temporal agreement is reflected
 460 in their high r values, with the DT2 returning $r \geq 0.87$ across all non-catalytic and catalytic cordwood
 461 tests, and the pDR returning $r \geq 0.79$. During the largest transient events, both instruments tend to over-
 462 predict relative to the reference. In the second catalytic cordwood high-burn (Figure 4, bottom-center), the
 463 DT2 and pDR report gravimetrically adjusted concentrations at the peak approaching 130 mg/m^3 while
 464 the reference peaks near 70 mg/m^3 , yet both instruments faithfully reproduce the shape and timing of the
 465 event. Bland–Altman plots (Figure S13) confirm this proportional bias increases with concentration. The
 466 first pellet high-burn (Figure 4, top-right) shows a similar pattern, with the DT2 and pDR reporting startup
 467 peaks roughly two to three times those of the reference, while still tracking the subsequent decay. Outside of
 468 these high-concentration transients, the optical instruments agree closely with the reference, suggesting that
 469 the over-prediction reflects the optical response to elevated loadings or shifts in particle optical properties
 470 (Figures S12 and S14).

471 The PP8306 tracks the general trend of the reference well for all catalytic cordwood heater tests ($r=0.83$ –
 472 0.98) and the high-burn test for the non-catalytic cordwood heater ($r=0.78$ and 0.84). The temporal tracking
 473 degraded during the low-burn phases of the non-catalytic cordwood heater, with r values of 0.45 and 0.66 .

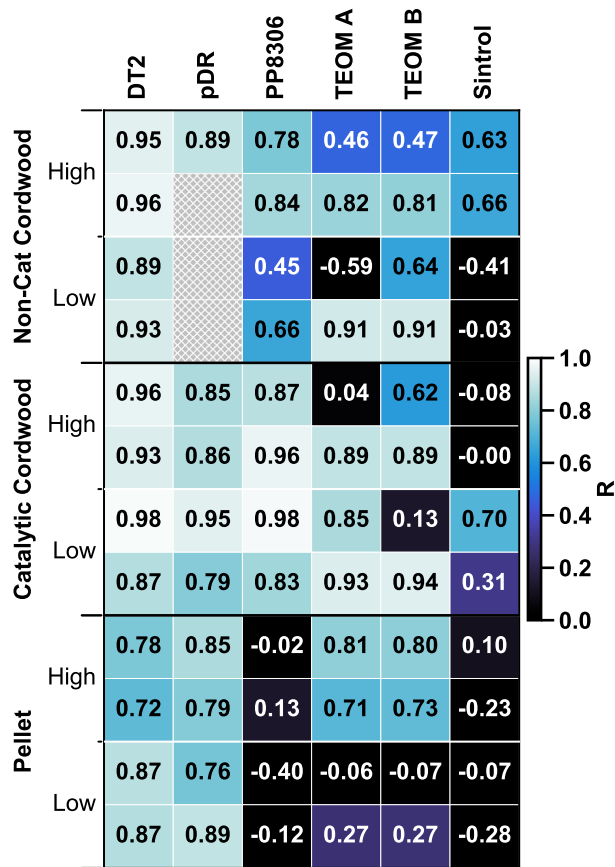


Figure 6: Pearson correlation coefficients (r) comparing gravimetrically-corrected real-time instruments to the reference mass concentration derived from size distribution measurements across heater types and operating conditions. pDR data was not collected for three of the non-catalytic cordwood tests due to user error.

474 This indicates that the instrument struggled to follow concentration fluctuations at lower emission levels.
475 Performance of the gravimetrically-adjusted PP8306 is poor across all pellet tests where the instrument does
476 not meaningfully track reference trends ($r = -0.40$ – 0.13). This is likely due to almost all of the PM mass
477 consisting of particles with diameters smaller than the instrument’s detection limit (300 nm), as discussed
478 in Section 3.1.

479 The TEOM, which was not adjusted by the reference filter, exhibits inconsistent temporal agreement that
480 varies by test and phase. During the second non-catalytic cordwood high-burn and both catalytic cordwood
481 low-burns, both channels return $r \geq 0.89$, indicating tight tracking of reference trends during moderate,
482 sustained emission events. However, temporal agreement can deteriorate following high-concentration tran-
483 sients, where the instrument signal drops sharply and can become strongly negative. The first non-catalytic
484 cordwood high-burn (Figure 4, top-left), for example, returns r values of 0.46 and 0.47 for both channels,
485 reflecting the TEOM’s failure to follow the reference during the initial high-emission period and the TEOM’s
486 subsequent oscillation through negative values. The most extreme measurement and disagreement between
487 channels that should be nominally equivalent occurred during the first catalytic cordwood high-burn, where
488 TEOM channel A shows concentrations as high as 1500 mg/m^3 shortly after the startup peak (Figure 4,
489 top-center), resulting in an r of 0.04 for that channel. These negative concentrations are also reflected in
490 the cumulative mass, where both channels overshoot the gravimetric reference during the startup and then
491 steadily lose mass for the remainder of the phase (Figure S10, top-left). During the pellet heater low-burn
492 phases, the TEOM signal frequently oscillates around zero and reports negative values, with both channels
493 returning negative r values for the first low burn.

494 The two channels also diverge from one another, as shown in the first non-catalytic cordwood low-burn.
495 With both channels nominally equivalent, this divergence is unexpected, particularly as the instrument
496 reported no errors or data quality flags during the experiment. The most extreme divergence occurs during
497 the first catalytic cordwood test (both high- and low-burn phases), which were conducted consecutively on
498 the same day. Subsequent review of the logged flow rate data revealed that flow rates on both channels
499 dropped by approximately 50% roughly 10 minutes after heater startup during the first catalytic cordwood
500 high-burn, coinciding with filter loading reaching $\sim 98\%$. According to the EPA-recommended standard
501 operating procedure, this flow rate excursion would constitute a failed measurement and invalidate the
502 affected data [43], yet no real-time indication of degraded data quality was provided by the instrument
503 during sampling. Flow rates returned to the nominal 1 LPM after both filters were changed at the end
504 of the high-burn phase. However, divergence between the channels persisted during the low-burn, with
505 channel B demonstrating poor temporal tracking ($r = 0.13$) and channel A tracking well ($r = 0.85$). These
506 results indicate that the flow excursion alone does not fully explain the observed artifacts, pointing instead

507 to the tapered-element measurement principle itself, where particle losses arise from mechanical shedding
508 of the oscillating filter or absorption and desorption of semi-volatile compounds on and off the collection
509 filter [3, 20, 37, 40, 50]. The artifacts observed here may be a fundamental consequence of applying the
510 TEOM outside its design regime, as the instrument was intended for slowly varying ambient aerosol rather
511 than the rapid, high concentration swings produced by a wood heater [57].

512 The Sintrol tracks moderately with the reference during the cordwood high-burns, with r values of 0.63
513 and 0.66 for the two non-catalytic cordwood high-burns. During the catalytic cordwood high-burns, the
514 Sintrol consistently shows a false increase in signal after engaging the catalyst around 10 minutes (Figure 4,
515 center column), yielding r values of -0.08 and -0.00 . The combined effect of under-reporting during
516 startup and the false post-catalyst peak produces the bow-tie pattern visible in the Bland–Altman plots
517 (Figure S23). The increase in signal did not correspond to temperature or humidity changes in the dilution
518 tunnel. Triboelectric instruments like the Sintrol are known to be sensitive to particle charge and composition,
519 both of which may have shifted following catalyst engagement. During the low-burn phases, the Sintrol r
520 values are near zero or negative across all heater types, indicating no meaningful temporal tracking. For the
521 pellet tests the Sintrol performs poorly across all phases, with r values ranging from -0.28 to 0.10 , indicating
522 the concentrations may be below its measurement limit.

523 3.3. Implications for Field Deployment

524 Although none of the instruments were investigated during in-situ measurement, several outcomes from
525 this laboratory study can help inform instrument selection and operational expectations for field deploy-
526 ment of real-time PM monitors in test facilities and in homes. The instrument’s suitability for field use
527 depends not only on measurement agreement but also on practical considerations such as setup complexity,
528 consumable requirements, portability, and the quality and timeliness of error reporting. Table 3 summarizes
529 each instrument’s operating principle, specifications, key operational observations, and tracking performance
530 obtained in this study, and the discussion below elaborates on each of these considerations.

531 *Measurement Agreement and Gravimetric Correction.* The suitability of each instrument depends heavily on
532 the intended application, as no single instrument performed well across all heater types, operating conditions,
533 and measurement goals. For applications requiring accurate integrated mass, the gravimetric mass ratios
534 reported without correction reveal that no optical instrument reliably reproduced the reference mass across
535 all conditions, with ratios ranging from 0.08 to 3.79 depending on instrument and phase. Gravimetric
536 correction reduced this variability but required co-located filter samples collected under the same conditions,
537 and correction factors were not stable across aerosol types or operating conditions. The optical instruments
538 require a co-located gravimetric filter to provide accurate mass measurements. In field settings where filter

539 changes are logistically difficult or where continuous unattended operation is required, this dependency on
540 consumable filters may limit the practicality of optical instruments for quantitative mass measurement. The
541 TEOM avoids this limitation as a direct mass instrument, but the data quality issues observed in this study
542 are concerning, and present additional practical barriers to field deployment. For applications requiring only
543 real-time trend tracking, such as identifying emission events or comparing relative performance across burn
544 conditions, the gravimetrically-corrected DT2 and pDR showed the most consistent temporal agreement
545 with the reference across heater types, with r values of 0.87–0.98 and 0.79–0.96 respectively. The Sintrol
546 showed the weakest temporal tracking overall ($r \leq 0.66$), and the TEOM showed the widest variability ($r =$
547 0.04–0.94), driven largely by the filter artifacts described in Section 3.2.

548 *Cost and Consumables.* Beyond measurement agreement, the instruments also differ in cost and consumable
549 requirements. The PP8306 is one of the least expensive instruments evaluated (tied with the Sintrol at \$5,000)
550 and additionally reports particle number concentration ($\# 1/\text{cm}^3$) along with calculated size-resolved particle
551 mass ($\text{PM}_{0.5}$, PM_1 , $\text{PM}_{2.5}$, PM_{10} , and total PM). The TEOM is the most expensive (\$25,000–\$40,000) and
552 is the only instrument providing a direct mass measurement, a method widely used in regulatory ambient
553 air monitoring. It should be noted that Thermo Scientific announced they plan to discontinue the 1405-D
554 TEOM in June 2026. The DT2 and pDR offer an integrated 37 mm filter (\$2.20 per filter) with no data-
555 collection delay following a filter change. The TEOM operates with two Pallflex TX40 13 mm filters (\sim \$40
556 each), which must be replaced at minimum before each test phase and potentially mid-phase during high-
557 PM events, which could result in data loss. After each filter change, the TEOM requires 5 to 10 minutes
558 before resuming data collection. The Sintrol contains no consumable parts but requires application-specific
559 calibration.

560 *Portability, Setup, and Error Reporting.* The DT2, pDR, and PP8306 are best suited for field measurements
561 owing to their smaller size and weight, battery-power option, and onboard data storage. The TEOM is
562 substantially larger and heavier than the optical instruments (roughly 24–72 times the volume and 7–18
563 times the weight), and requires AC power. While most instruments required less than 15 minutes to set
564 up with no specialized training, the TEOM setup required an expert user approximately one hour, with
565 post-test data validation and processing requiring additional expertise.

566 The DT2 and PP8306 display error messages on screen when a fault is detected, while the pDR freezes the
567 display on the last recorded value without an explicit alert. The TEOM reports status and error codes on its
568 front panel, but the indicators do not include real-time warnings of degraded data quality during sampling.
569 For example, the flow rate excursion observed during the first catalytic cordwood high-burn (Figure 4) was
570 only identifiable through post-hoc review of logged flow data by a trained expert. Since real-time indication of

571 measurement failure is not available to the operator, data that would constitute a failed measurement under
572 EPA-recommended procedures may not be identified until after the test is complete [43]. Less experienced
573 users may therefore face an even greater risk of undetected measurement failures. The Sintrol provides only
574 a rudimentary LED status indicator, with two states relevant to field use: Normal Operation (solid green)
575 and FAULT (blinking red), where FAULT indicates no valid signal is being generated. Normal Operation
576 does not differentiate between reliable and unreliable signals, meaning conditions such as concentrations
577 below the detection limit or interference from catalyst engagement will not trigger any alert, as was observed
578 during this study.

Table 3: Overview of particulate instruments evaluated.

	DustTrak II 8530	pDR-1500	Particles Plus 8306	1405-D TEOM^a	Sintrol S203
Operational notes	Robust; setup <15 min; briefly exceeded max conc. at startup	Robust; setup <15 min; no data for 3 tests due to sampling line disturbance	Compact; PM mass and size; setup <15 min; requires additional dilution beyond dilution tunnel	Setup >1 hr; observed filter mass-loss and sustained negative cumulative mass	Best for direct stack measurement; setup <15 min; requires application specific calibration
Pearson Correlation (r) ^b	0.87–0.98	0.79–0.96	–0.33–0.96	–0.59–0.94	–0.41–0.70
Gravimetric mass ratio ^c	0.63–1.00 (filter) 0.30–3.79 (optical)	0.08–1.54	0.09–1.14	0.06–1.07	N/A
Operating principle	Optical	Optical	Optical	Mass (TEOM)	Triboelectric
Conc. range (mg/m ³)	0.001–400	0.001–400	0.00001–20	0–1000	0.01–>1000
Form factor	13.5×21.6×22.4 cm; 1.6–2.5 kg; battery	18.1×14.3×8.4 cm; 1.2 kg; battery	13.0×10.8×31.1 cm; 1.0 kg; battery	43.2×48.3×75 cm; 18 kg; AC only	65.6×16.8×17.5 cm; 1.5 kg; AC only
Data acquisition ^d	1 s native; 60,000 samples internal; streaming	1 s native; 500,000 samples internal; streaming	1 s native; 45,000 samples internal; streaming	10 s native; 500,000 samples internal; streaming	Not stated; PC log only; streaming
Approx. cost (USD) ^e	\$8,600	\$10,000	\$5,000	\$25,000–40,000	\$5,000
Gravimetric correction	Required; integrated 37 mm filter	Required; integrated 37 mm filter	Required; external filter	Not required (direct mass)	N/A (TSP only)
Per-test consumables ^f	\$2.20/filter; no resumption delay	\$2.20/filter; no resumption delay	External filter; no resumption delay	~\$80/test (2 filters); 5–10 min resumption after change	None
Zero calibration	Yes (user)	Yes (user)	Zero check only	Not available	Zero check only

^a Thermo Scientific will discontinue the 1405-D TEOM on June 30, 2026.^b Pearson correlation coefficient (r) calculated from 10-s averaged data. TEOM r represents the best performing channel per phase.^c Ratio of instrument-integrated mass to the gravimetric filter reference across all tests and phases, where 1.0 indicates perfect agreement. Values are reported without gravimetric correction. TEOM range represents the best performing channel per phase.^d Native measurement interval; internal storage capacity; streaming capability.^e Estimated 2026 USD; see Table S10 for full breakdown including consumables.^f Approximate cost of consumable filters per test phase and time required for instrument to resume data collection after a filter change.

579 4. Conclusions

580 The purpose of this study was to evaluate five continuous PM instruments against gravimetric filter
581 references and size-resolved reference concentrations across three residential wood heater types and two op-
582 erating phases, with the goal of informing instrument selection for laboratory test facilities and potential field
583 deployment. Overall, no single instrument performed well across all heater types, operating conditions, and
584 measurement goals, and instrument selection necessarily involves tradeoffs between mass accuracy, temporal
585 resolution, and practical deployability.

586 The results demonstrate that neither optical nor direct-mass measurement principles are well-matched
587 to the full range of conditions produced by residential wood heaters. Optical instruments are fundamentally
588 constrained by the mismatch between their calibration aerosols and wood smoke aerosol. For some heaters
589 and operating conditions, a substantial fraction of particle mass may fall below the instruments' size detection
590 limit, rendering it effectively invisible to optical monitors. Condition-specific gravimetric correction factors
591 were also not stable across fuel types or operating conditions, suggesting they cannot be assumed to transfer
592 reliably between fuel or heater types. The TEOM, despite providing direct mass measurement without
593 gravimetric correction, performed poorly during cordwood combustion, where the rapid, high-concentration
594 transients produced conditions outside its design regime and introduced a risk of undetected measurement
595 failure. For applications requiring real-time trend tracking rather than absolute mass, the DT2 and pDR
596 outperformed both the TEOM and the PP8306. This suggests that more complex instruments do not
597 necessarily perform better for wood heater PM monitoring.

598 Several instruments show strong promise for specific heaters and operating conditions; however, further
599 research is needed to evaluate instrument performance across a broader range of stove types, operating
600 conditions, wood species, and moisture contents. Concurrent black carbon measurements in future studies
601 would help clarify how shifts in aerosol composition drive instrument-specific biases across fuel types and
602 burn conditions. Opacity sensors represent a further avenue for investigation, as they may reduce reliance
603 on dilution tunnels; however, they would still require calibration to relate opacity to PM mass.

604 **CRedit authorship contribution statement**

605 **VHR:** Conceptualization, Formal Analysis, Funding Acquisition, Investigation, Methodology, Project
606 Administration, Supervision, Validation, Visualization, Writing – Original Draft, Writing – Review & Edit-
607 ing. **BCS:** Conceptualization, Funding Acquisition, Validation, Writing – Original Draft, Writing – Review
608 & Editing. **RT:** Formal Analysis, Investigation, Methodology, Validation, Visualization, Writing – Original
609 Draft, Writing – Review & Editing. **SSC:** Investigation, Validation, Visualization, Writing – Original Draft,

610 Writing – Review & Editing. **DAB**: Investigation, Validation, Visualization, Writing – Original Draft, Writing – Review & Editing. **WD**: Conceptualization, Investigation, Validation, Writing – Review & Editing.
 611 ing – Review & Editing. **WD**: Conceptualization, Investigation, Validation, Writing – Review & Editing.
 612 **EA**: Conceptualization, Funding Acquisition, Supervision, Validation, Writing – Review & Editing. **JC**:
 613 Conceptualization, Funding Acquisition, Supervision, Validation, Writing – Review & Editing.

614 **Declaration of Generative AI and AI-Assisted Technologies in the Writing Process**

615 During the preparation of this work, the author(s) used the CBorg AI platform provided by the IT
 616 Division at the Lawrence Berkeley National Laboratory (Supported by the Director, Office of Science, Office
 617 of Basic Energy Sciences, of the U.S. Department of Energy under Contract No. DE-AC02-05CH11231) to
 618 improve language clarity, readability, and to assist with the structural proofreading of the manuscript text.
 619 After using this tool, the authors reviewed and edited the content as needed and take full responsibility for
 620 the final content of the publication.

621 **Acknowledgments**

622 The work described in this study was conducted at Lawrence Berkeley National Laboratory and supported
 623 by the U.S. Department of Energy Bioenergy Technologies Office under Contract No. DE-AC02-05CH11231.

624 This research used the CBorg AI platform and resources provided by the IT Division at the Lawrence
 625 Berkeley National Laboratory (Supported by the Director, Office of Science, Office of Basic Energy Sciences,
 626 of the U.S. Department of Energy under Contract No. DE-AC02-05CH11231). CBorg was used to assist in
 627 engineering and data-handling tasks during the research process. This included generating scripts for logging
 628 data from new instruments, integrating those scripts into our existing data acquisition infrastructure, refining
 629 the cosmetic features of figures, and debug code. All code and results were reviewed, tested, and verified by
 630 the authors. The authors also acknowledge the use of Google’s NotebookLM to assist in reviewing literature
 631 identified by the authors. The tool was utilized strictly to query published literature databases created by
 632 the authors and cross-reference our data-driven arguments against existing academic precedents.

633 The authors gratefully acknowledge Mark Shmorhun for project oversight, support, and technical review.
 634 We also thank our industry partners for their valuable contributions: Chris Neufeld and Corie Podschelne
 635 for providing test equipment and technical guidance.

References

- [1] Alfano, B., Barretta, L., Del Giudice, A., De Vito, S., Di Francia, G., Esposito, E., Formisano, F.,
 Massera, E., Miglietta, M.L., Polichetti, T., . A review of low-cost particulate matter sensors from

- the developers' perspectives. *Sensors* 20, 6819. URL: <https://www.mdpi.com/1424-8220/20/23/6819>, doi:10.3390/s20236819.
- [2] Allen, G., Morin, B., Ahmadi, M., Rector, L., a. Online measurement of pm from residential wood heaters in a dilution tunnel. *Journal of the Air & Waste Management Association* 72, 662–678. URL: <https://www.tandfonline.com/doi/full/10.1080/10962247.2022.2049927>, doi:10.1080/10962247.2022.2049927.
- [3] Allen, G., Sioutas, C., Koutrakis, P., Reiss, R., Lurmann, F.W., Roberts, P.T., b. Evaluation of the TEOM[®] method for measurement of ambient particulate mass in urban areas. *Journal of the Air & Waste Management Association* 47, 682–689. URL: <https://www.tandfonline.com/doi/full/10.1080/10473289.1997.10463923>, doi:10.1080/10473289.1997.10463923.
- [4] ASTM International, a. ASTM E2515-11 Test Method for Determination of Particulate Matter Emissions Collected by a Dilution Tunnel. Technical Report E2515-11. ASTM International. URL: <http://www.astm.org/cgi-bin/resolver.cgi?E2515-11R17>, doi:10.1520/E2515-11R17.
- [5] ASTM International, b. ASTM E2618-13 Standard Test Method for Measurement of Particulate Emissions and Heating Efficiency of Solid Fuel-Fired Hydronic Heating Appliances. Technical Report E2618-13. ASTM International. URL: <https://www.astm.org/e2618-13r19.html>.
- [6] ASTM International, c. ASTM E2779-10 Test Method for Determining Particulate Matter Emissions from Pellet Heaters. Technical Report E2779-10. ASTM International. URL: <http://www.astm.org/cgi-bin/resolver.cgi?E2779-10R17>, doi:10.1520/E2779-10R17.
- [7] ASTM International, d. ASTM E2780-10 Test Method for Determining Particulate Matter Emissions from Wood Heaters. Technical Report E2780-10. ASTM International. URL: <http://www.astm.org/cgi-bin/resolver.cgi?E2780-10R17>, doi:10.1520/E2780-10R17.
- [8] ASTM International, e. ASTM E3053-18e2 Standard Test Method for Determining Particulate Matter Emissions from Wood Heaters Using Cordwood Test Fuel. Technical Report E3053-18e2. ASTM International. URL: <http://www.astm.org/cgi-bin/resolver.cgi?E3053-17>, doi:10.1520/E3053-17.
- [9] ASTM International, f. Test Methods for Direct Moisture Content Measurement of Wood and Wood-Based Materials. Technical Report. ASTM International. URL: <http://www.astm.org/cgi-bin/resolver.cgi?D4442-20>, doi:10.1520/D4442-20.
- [10] Bioenergy International, 2022. DOE selects six projects to advance US wood heaters. Technical Report. Bioenergy International. Published: April 14, 2022. Accessed: May 22, 2026.

- [11] Bland, J.M., Altman, D.G., 2007. Agreement Between Methods of Measurement with Multiple Observations Per Individual. *Journal of Biopharmaceutical Statistics* 17, 571–582. URL: <https://www.tandfonline.com/doi/full/10.1080/10543400701329422>, doi:10.1080/10543400701329422.
- [12] Boman, C., Pettersson, E., Westerholm, R., Boström, D., Nordin, A., . Stove performance and emission characteristics in residential wood log and pellet combustion, part 1: Pellet stoves. *Energy & Fuels* 25, 307–314. URL: <https://pubs.acs.org/doi/10.1021/ef100774x>, doi:10.1021/ef100774x.
- [13] Brandelet, B., Rose, C., Landreau, J., Druette, L., Rogaume, Y., . Toward a cleaner domestic wood heating by the optimization of firewood stoves? *Journal of Cleaner Production* 325, 129338. URL: <https://linkinghub.elsevier.com/retrieve/pii/S095965262103523X>, doi:10.1016/j.jclepro.2021.129338.
- [14] Butcher, T., Trojanowski, R., 2020. Effect of thermal storage on the emissions and efficiency performance of a wood pellet-fired residential boiler. *ACS Omega* 5. URL: <https://www.osti.gov/biblio/1668663>, doi:10.1021/acsomega.0c03080.
- [15] Båfver, L.S., Leckner, B., Tullin, C., Berntsen, M., 2011. Particle emissions from pellets stoves and modern and old-type wood stoves. *Biomass and Bioenergy* 35, 3648–3655. doi:<https://doi.org/10.1016/j.biombioe.2011.05.027>.
- [16] Caubel, J., Trojanowski, R., Butcher, T., Rapp, V., 2023. A review of regulatory standard test methods for residential wood heaters and recommendations for their advancement. *Renewable and Sustainable Energy Reviews* 184, 113501. URL: <https://linkinghub.elsevier.com/retrieve/pii/S1364032123003581>, doi:10.1016/j.rser.2023.113501.
- [17] Chandrasekaran, S.R., Laing, J.R., Holsen, T.M., Raja, S., Hopke, P.K., . Emission characterization and efficiency measurements of high-efficiency wood boilers. *Energy & Fuels* 25, 5015–5021. URL: <https://pubs.acs.org/doi/10.1021/ef2012563>, doi:10.1021/ef2012563.
- [18] Charron, A., . Quantitative interpretation of divergence between PM10 and PM2.5 mass measurement by TEOM and gravimetric (partisol) instruments. *Atmospheric Environment* 38, 415–423. URL: <https://linkinghub.elsevier.com/retrieve/pii/S1352231003008616>, doi:10.1016/j.atmosenv.2003.09.072.
- [19] CSA Group, . CSA B415.1:22 Performance testing of solid-biofuel-burning heating appliances. Technical Report CSA B415.1:22. CSA Group. URL: <https://www.csagroup.org/store/product/2701332/>.

- [20] DeCarlo, P.F., Slowik, J.G., Worsnop, D.R., Davidovits, P., Jimenez, J.L., . Particle morphology and density characterization by combined mobility and aerodynamic diameter measurements. part 1: Theory. *Aerosol Science and Technology* 38, 1185–1205. URL: <http://www.tandfonline.com/doi/abs/10.1080/027868290903907>, doi:10.1080/027868290903907.
- [21] Delmhorst, 2011. Delmhorst BD2100 User Manual 510INS-0006 Rev. 01/11. URL: <https://www.emlab.com/m/store/Delmhorst%20BD2100%20User%20Manual.pdf>.
- [22] Despotović, v.V., 2013. Some Experiences in the Exploitation of Triboelectric Sensors for Measuring Concentration of Particulate Matter on Thermal Power Plants. URL: https://www.viser.edu.rs/uploads/2020/03/TES-2_Z.Despotovic_INFOTEH_2013.pdf. presented at INFOTEH-JAHORINA 2013, Paper Ref: TES-2.
- [23] European Committee for Standardization, . EN 16510-1:2022 Residential solid fuel burning appliances. Part 1: General requirements and test methods. Technical Report EN 16510-1:2022. European Committee for Standardization. URL: <https://www.en-standard.eu/bs-en-16510-1-2022-residential-solid-fuel-burning-appliances-general-requirements-and-test-methods>.
- [24] Fachinger, F., Drewnick, F., Gieré, R., Borrmann, S., . How the user can influence particulate emissions from residential wood and pellet stoves: Emission factors for different fuels and burning conditions. *Atmospheric Environment* 158, 216–226. URL: <https://linkinghub.elsevier.com/retrieve/pii/S1352231017301590>, doi:10.1016/j.atmosenv.2017.03.027.
- [25] Giavarina, D., 2015. Understanding Bland Altman analysis. *Biochimica Medica* 25, 141–151. URL: <http://www.biochimica-medica.com/en/journal/25/2/10.11613/BM.2015.015>, doi:10.11613/BM.2015.015.
- [26] Hagan, D.H., Kroll, J.H., 2020. Assessing the accuracy of low-cost optical particle sensors using a physics-based approach. *Atmospheric Measurement Techniques* 13, 6343–6355. URL: <https://amt.copernicus.org/articles/13/6343/2020/>, doi:10.5194/amt-13-6343-2020.
- [27] Hand, J.L., Kreidenweis, S.M., . A new method for retrieving particle refractive index and effective density from aerosol size distribution data. *Aerosol Science and Technology* 36, 1012–1026. URL: <http://www.tandfonline.com/doi/abs/10.1080/02786820290092276>, doi:10.1080/02786820290092276.
- [28] Hauck, H., Berner, A., Gomiscek, B., Stopper, S., Puxbaum, H., Kundi, M., Preining, O., . On the equivalence of gravimetric PM data with TEOM and beta-attenuation measurements. *Journal of Aerosol Sci-*

- ence 35, 1135–1149. URL: <https://linkinghub.elsevier.com/retrieve/pii/S0021850204000667>, doi:10.1016/j.jaerosci.2004.04.004.
- [29] International Organization for Standardization, 2018. Determination of particle size distribution — Light scattering airborne particle counter for clean spaces. Standard ISO 21501-4:2018. International Organization for Standardization. Geneva, Switzerland. URL: iso.org.
- [30] Kingham, S., Durand, M., Aberkane, T., Harrison, J., Gaines Wilson, J., Epton, M., . Winter comparison of TEOM, MiniVol and DustTrak PM10 monitors in a woodsmoke environment. *Atmospheric Environment* 40, 338–347. URL: <https://linkinghub.elsevier.com/retrieve/pii/S1352231005008885>, doi:10.1016/j.atmosenv.2005.09.042.
- [31] Kinsey, J.S., Kariher, P.H., Dong, Y., . Evaluation of methods for the physical characterization of the fine particle emissions from two residential wood combustion appliances. *Atmospheric Environment* 43, 4959–4967. URL: <https://linkinghub.elsevier.com/retrieve/pii/S1352231009005895>, doi:10.1016/j.atmosenv.2009.07.008.
- [32] Kortekand, M., de Vries, J., van Berkel, P., de Bruyn, S., 2022. Health-related social costs of air pollution due to residential heating and cooking in the EU27 and UK. Report 22.190144.027. CE Delft. URL: <https://cedelft.eu/publications/health-related-social-costs-of-air-pollution-due-to-residential-heating-and-cooking-in-the-eu27-and-uk>
- [33] Kortelainen, M., Jokiniemi, J., Tiitta, P., Tissari, J., Lamberg, H., Leskinen, J., Grigonyte-Lopez Rodriguez, J., Koponen, H., Antikainen, S., Nuutinen, I., Zimmermann, R., Sippula, O., . Time-resolved chemical composition of small-scale batch combustion emissions from various wood species. *Fuel* 233, 224–236. URL: <https://linkinghub.elsevier.com/retrieve/pii/S0016236118311049>, doi:10.1016/j.fuel.2018.06.056.
- [34] Krieger, U.K., Rupp, S., Hausammann, E., Peter, T., 2007. Simultaneous measurements of pm10 and pm1 using a single teom. *Aerosol Science and Technology* 41, 975–980. doi:10.1080/02786820701639715.
- [35] Kulkarni, P., Baron, P.A., Willeke, K., 2011. *Aerosol Measurement: Principles, Techniques, and Applications*. 3rd ed ed., John Wiley & Sons, Incorporated, Hoboken.
- [36] Levin, E.J.T., McMeeking, G.R., Carrico, C.M., Mack, L.E., Kreidenweis, S.M., Wold, C.E., Moosmüller, H., Arnott, W.P., Hao, W.M., Collett, J.L., Malm, W.C., 2010. Biomass burning smoke aerosol

- properties measured during fire laboratory at missoula experiments (FLAME). *Journal of Geophysical Research: Atmospheres* 115, 2009JD013601. URL: <https://agupubs.onlinelibrary.wiley.com/doi/10.1029/2009JD013601>, doi:10.1029/2009JD013601.
- [37] Li, Q.F., Wang-Li, L., Liu, Z., Heber, A.J., . Field evaluation of particulate matter measurements using tapered element oscillating microbalance in a layer house. *Journal of the Air & Waste Management Association* 62, 322–335. URL: <https://www.tandfonline.com/doi/full/10.1080/10473289.2011.650316>, doi:10.1080/10473289.2011.650316.
- [38] Lin, L.I.K., 1989. A Concordance Correlation Coefficient to Evaluate Reproducibility. *Biometrics* 45, 255. URL: <https://www.jstor.org/stable/2532051?origin=crossref>, doi:10.2307/2532051.
- [39] Martin Bland, J., Altman, D., 1986. Statistical Methods for Assessing Agreement Between Two Methods of Clinical Measurement. *The Lancet* 327, 307–310. URL: <https://linkinghub.elsevier.com/retrieve/pii/S0140673686908378>, doi:10.1016/S0140-6736(86)90837-8.
- [40] Mignacca, D., Stubbs, K., . Effects of equilibration temperature on PM₁₀ concentrations from the TEOM method in the lower fraser valley. *Journal of the Air & Waste Management Association* 49, 1250–1254. URL: <https://www.tandfonline.com/doi/full/10.1080/10473289.1999.10463914>, doi:10.1080/10473289.1999.10463914.
- [41] Misiulia, D.I., Kuz'min, V.V., Markov, V.A., . Developing an untwisting device for cyclones and estimating its parameters. *Theoretical Foundations of Chemical Engineering* 47, 274–283. URL: <https://link.springer.com/10.1134/S004057951303007X>, doi:10.1134/S004057951303007X.
- [42] Moosmüller, H., Arnott, W.P., Rogers, C.F., Bowen, J.L., Gillies, J.A., Pierson, W.R., Collins, J.F., Durbin, T.D., Norbeck, J.M., 2001. Time resolved characterization of diesel particulate emissions. 1. instruments for particle mass measurements. *Environmental Science & Technology* 35, 781–787. doi:10.1021/es0013935.
- [43] New York State Energy Research and Development Authority, 2025. NYSERDA Standard Operation Procedures for use of a Thermo Scientific 1405-D TEOM in a dilution tunnel with wood-fired stoves, hydronic heaters, and furnaces with calculations for grams PM emitted for EPA Independent Assessment Project. Standard Operating Procedure EPA-HQ-OAR-2016-0130-0076. New York State Energy Research and Development Authority (NYSERDA). URL: <https://www.regulations.gov/document/EPA-HQ-OAR-2016-0130-0076>. submitted to EPA docket EPA-HQ-OAR-2016-0130. Accessed 2026-05-14.

- [44] Ouimette, J.R., Malm, W.C., Schichtel, B.A., Sheridan, P.J., Andrews, E., Ogren, J.A., Arnott, W.P., . Evaluating the PurpleAir monitor as an aerosol light scattering instrument. *Atmospheric Measurement Techniques* 15, 655–676. URL: <https://amt.copernicus.org/articles/15/655/2022/>, doi:10.5194/amt-15-655-2022.
- [45] Particles Plus, Inc., 2019. 8000 Series Handheld Particle Counters User’s Manual. Particles Plus, Inc.. Stoughton, MA, USA. URL: <https://www.particlesplus.com>. copyright 2019 by Particles Plus, Inc.
- [46] Rapp, V.H., Caubel, J.J., Wilson, D.L., Gadgil, A.J., 2016. Reducing Ultrafine Particle Emissions Using Air Injection in Wood-Burning Cookstoves. *Environmental Science & Technology* 50, 8368–8374. URL: <https://pubs.acs.org/doi/10.1021/acs.est.6b01333>, doi:10.1021/acs.est.6b01333.
- [47] Rapp, V.H., Chen, S.S., Anacleto-Black, D., Putaansuu, N., . Evaluation of a Smoke Opacity Sensor for Improving Residential Wood Heater Combustion. Technical Report LBNL-2001749. LBNL. URL: <https://escholarship.org/uc/item/4250w1jg>, doi:10.20357/B79G77.
- [48] Roessler, D.M., Faxvog, F.R., 1979. Opacity of black smoke: calculated variation with particle size and refractive index. *Applied Optics* 18, 1399. URL: <https://opg.optica.org/abstract.cfm?URI=ao-18-9-1399>, doi:10.1364/AO.18.001399.
- [49] SAE International, 2018. J1667-201802 Snap acceleration smoke test procedure for heavy-duty diesel powered vehicles. Technical Report. SAE International. URL: https://www.sae.org/standards/j1667_201802-snap-acceleration-smoke-test-procedure-heavy-duty-diesel-powered-vehicles, doi:10.4271/J1667_201802.
- [50] Salvador, C.M., Chou, C.C.K., . Analysis of semi-volatile materials (SVM) in fine particulate matter. *Atmospheric Environment* 95, 288–295. URL: <https://linkinghub.elsevier.com/retrieve/pii/S1352231014004920>, doi:10.1016/j.atmosenv.2014.06.046.
- [51] Schön, C., Hartmann, H., 2018. Status of PM emission measurement methods and new developments. Technical Report. IEA Bioenergy. Task 32.
- [52] Schwab, J.J., Spicer, J., Demerjian, K.L., Ambs, J.L., Felton, H.D., . Long-term field characterization of tapered element oscillating microbalance and modified tapered element oscillating microbalance samplers in urban and rural new york state locations. *Journal of the Air & Waste Management Association* 54, 1264–1280. URL: <https://www.tandfonline.com/doi/full/10.1080/10473289.2004.10470998>, doi:10.1080/10473289.2004.10470998.

- [53] Seabold, S., Perktold, J., 2010. Statsmodels: Econometric and Statistical Modeling with Python, in: SciPy Proceedings, Austin, Texas. pp. 92–96. URL: <https://doi.curvenote.com/10.25080/Majora-92bf1922-011>, doi:10.25080/Majora-92bf1922-011.
- [54] Singer, B.C., Delp, W.W., . Response of consumer and research grade indoor air quality monitors to residential sources of fine particles. *Indoor Air* 28, 624–639. URL: <https://onlinelibrary.wiley.com/doi/10.1111/ina.12463>, doi:10.1111/ina.12463.
- [55] Sintrol Oy, 2023. S200 Series Dust Monitors User Manual: Models S201 and S203. Sintrol Oy. Helsinki, Finland. URL: <https://sintrol.com>. revision 6, Publication date: 2023-06-07.
- [56] Standards Australia, Standards New Zealand, 2014. AS/NZS 4013:2014 Domestic solid fuel burning appliances—Method for determination of flue gas emission. Standard. Standards Australia and Standards New Zealand. Sydney, NSW and Wellington, NZ.
- [57] Sullivan, B., Allawatt, G., Emery, A., Means, P., Kramlich, J., Posner, J., . Time-resolved particulate emissions monitoring of cookstove biomass combustion using a tapered element oscillating microbalance. *Combustion Science and Technology* 189, 923–936. URL: <https://www.tandfonline.com/doi/full/10.1080/00102202.2016.1253564>, doi:10.1080/00102202.2016.1253564.
- [58] Thermo Fisher Scientific, . TEOM 1405-D Dichotomous Ambient Particulate Monitor Operator’s Manual. Environmental Instruments Division. URL: <http://tools.thermofisher.com/content/sfs/manuals/EPM-TEOM1405D-Manual.pdf>.
- [59] Thermo Fisher Scientific, 2022. MIE pDR-1500 Active Personal Particulate Monitor Instruction Manual. Air Quality Instruments. Franklin, MA, USA. URL: <https://www.thermofisher.com>. part Number 105983-00.
- [60] Thielke, J.F., Pilat, M.J., 1978. Plume opacity related to particle mass concentration and size distribution. *Atmospheric Environment* (1967) 12, 2439–2447. URL: <https://linkinghub.elsevier.com/retrieve/pii/0004698178902883>, doi:10.1016/0004-6981(78)90288-3.
- [61] Trojanowski, R., 2025. A Comparison of Novel Woodstove Catalytic Combustors to Improve Low Temperature Light off and Catalyst Stability at High Temperatures and Corrosive Environments, Including Stability of Catalytic Combustors used in Coastal Environments. Technical Report. Brookhaven National Laboratory (BNL), Upton, NY (United States); Applied Ceramics Inc., Atlanta, GA (United States). URL: <https://www.osti.gov/biblio/2572567>, doi:10.2172/2572567.

- [62] Trojanowski, R., Fthenakis, V., 2019. Nanoparticle emissions from residential wood combustion: A critical literature review, characterization, and recommendations. *Renewable and Sustainable Energy Reviews* 103, 515–528. URL: <https://linkinghub.elsevier.com/retrieve/pii/S1364032119300012>, doi:10.1016/j.rser.2019.01.007.
- [63] TSI Incorporated, 2012. DustTrak II Aerosol Monitor Theory of Operation. Application Note EXPMN-001, Rev. C. TSI Incorporated. Shoreview, MN, USA. Printed in U.S.A.
- [64] TSI Incorporated, 2023. Model 8530/8530EP/8532 DustTrak II Aerosol Monitor Operation and Service Manual. TSI Incorporated. Shoreview, MN, USA. URL: <https://www.tsi.com/p/N6001893>, Revision W.
- [65] U.S. Department of Energy, 2025. U.S. Department of Energy Selects Three Projects to Advance Wood Heater Innovation to Access Affordable, Renewable Energy. Technical Report. U.S. Department of Energy. Office of Energy Efficiency and Renewable Energy, Bioenergy Technologies Office. Published: January 16, 2025. Accessed: May 22, 2026.
- [66] U.S. Energy Information Administration, 2023. Table CE7.2: Household Wood Consumption in the United States—Totals and Averages, 2020. 2020 Residential Energy Consumption Survey (RECS). U.S. Department of Energy, Office of Energy Consumption and Efficiency Statistics. URL: <https://www.eia.gov/consumption/residential/data/2020/index.php?view=consumption>.
- [67] U.S. Environmental Protection Agency, . ALT-140 Approval of Integrated Duty Cycle Test Method (IDC) for Subpart AAA Wood Heater Compliance Testing. Technical Report ALT-140. U.S. Environmental Protection Agency. URL: https://www.epa.gov/system/files/documents/2021-07/atm_14_2.pdf.
- [68] U.S. Environmental Protection Agency, 2020. Method 5 –Determination of Particulate Matter Emissions from Stationary Sources. Federal Test Method 40 CFR Part 60, Appendix A-3. U.S. EPA Air Emission Measurement Center (EMC). URL: <https://www.epa.gov/emc/method-5-particulate-matter-pm>. promulgated December 7, 2020.
- [69] Wang, K., Nakao, S., Thimmaiah, D., Hopke, P.K., a. Emissions from in-use residential wood pellet boilers and potential emissions savings using thermal storage. *Science of The Total Environment* 676, 564–576. URL: <https://linkinghub.elsevier.com/retrieve/pii/S0048969719318601>, doi:10.1016/j.scitotenv.2019.04.325.

- [70] Wang, X., Robbins, C., Hoekman, S.K., Chow, J.C., Watson, J.G., Schuetzle, D., b. Dilution sampling and analysis of particulate matter in biomass-derived syngas. *Frontiers of Environmental Science & Engineering in China* 5, 320–330. URL: <http://link.springer.com/10.1007/s11783-011-0347-x>, doi:10.1007/s11783-011-0347-x.
- [71] Wang, X., Watson, J.G., Chow, J.C., Gronstal, S., Kohl, S.D., c. An efficient multipollutant system for measuring real-world emissions from stationary and mobile sources. *Aerosol and Air Quality Research* 12, 145–160. URL: <https://aaqr.org/articles/aaqr-11-11-0a-0187>, doi:10.4209/aaqr.2011.11.0187.

Supplementary Data for Evaluating real-time particulate matter instruments against gravimetric and size-resolved references to advance residential wood heater development

Vi H. Rapp, Brett C. Singer, Rebecca Trojanowski, Sharon S. Chen, Dylan Anacleto-Black, Willaim W.

Delp, Eric Adair, and John Crouch

S-1. Supporting Methods

S-1.1. Secondary Dilution System

Table S1: Summary of dilution tunnel and secondary dilution system flow metrics across test phases.

Phase	Dilution Tunnel Flow Rate	Secondary Dilution Sample Flow Rate	Secondary Dilution Air Flow Rate	Secondary Dilution Factor (phase-average)
Cordwood High	500 SCFM	1.2 SLPM	43.2 SLPM	38
Cordwood Low	500 SCFM	3.0–5.2 SLPM	10.2–36.0 SLPM	3–13
Cat. Cordwood High	500 SCFM	1.3 SLPM	43.2 SLPM	36
Cat. Cordwood Low	500 SCFM	1.2–5.1 SLPM	10.4–16.9 SLPM	3–15
Pellet High	300 SCFM	2.9 SLPM	42 SLPM	15
Pellet Low	300 SCFM	3.2 SLPM	12.4 SLPM	5

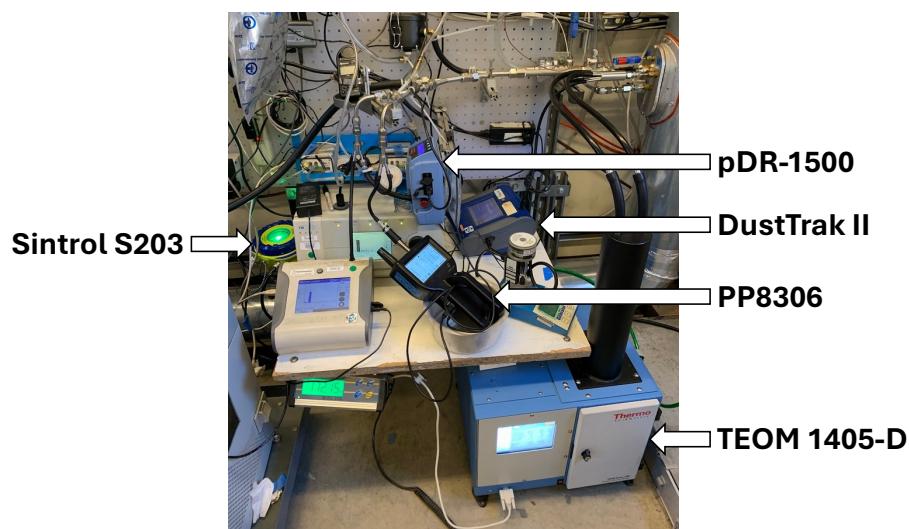


Figure S1: Image of sampling lines from dilution tunnel, secondary dilution system, and particle instruments.

S-1.2. Chimney Specifications

Chimney dimensions and total heights for each heater are summarized in Table S2. Each chimney comprised single-wall stove pipe topped with 1-inch (2.54 cm) double-wall insulated pipe, with a stove-pipe connector at the base where required. The pellet heater’s rear-facing exhaust port required a single-wall tee connector to route the chimney upward; the physical heater itself was 0.87 m (34.125 in.) tall, though this dimension does not contribute to the total stack height since the exhaust exits from the rear.

Table S2: Heights of heaters and stack components. Total height is measured from the top of the scale to the top of the chimney.

	Cordwood	Catalytic-Cordwood	Pellet
Chimney Diameter (internal)	15.24 cm (6 in.)	15.24 cm (6 in.)	10.16 cm (4 in.)
Scale to Stack Base ^a	0.81 m (31.875 in.)	0.77 m (30.5 in.)	0.51 m (20.25 in.)
Stove-pipe Connector	7.62 cm (3 in.)	—	12.7 cm (5 in.) ^b
Single-wall Stove Pipe	1.63 m (64 in.)	1.63 m (64 in.)	1.68 m (66 in.)
Insulated Chimney	2.11 m (83 in.)	2.11 m (83 in.)	2.03 m (80 in.)
Total Height	4.62 m (181.875 in.)	4.51 m (177.5 in.)	4.35 m (171.25 in.)

^a For the cordwood and catalytic-cordwood heaters, this is the heater height, since the stack rises from the top of the heater. For the pellet heater, this is the distance from the scale to the center of the rear-facing exhaust port.

^b Single-wall tee connector used to route the rear-facing exhaust upward.

S-1.3. Heater Operating Procedures

Figures S2 through S7 show the fuel loads and air control settings for each heater and operating phase. A detailed description of the high-burn and low-burn procedures are provided in Tables S3 and S4.

Table S3: High-burn operating protocol for the three heater types. All high-burn phases begin with a cold (room-temperature) firebox, cleaned of ash from previous burns. Times in the Events column are minutes from ignition (cordwood, cat-cordwood) or from power-on (pellet).

Heater	Initial Fuel Load	Initial Settings	Events (time: action)	Duration (min)
Cordwood	100 g paper knots, 1.0 kg kindling, 1.2–1.4 kg small logs; door open	Burn Rate Air Control = 5; Automatic Combustion Control (ACC) lever = “HI”	0–1: lighting; 3–5: (optional) shut door; 5–8: load 2 small logs (1.6–1.9 kg); 6–9: shut door; 19–20: load 2–4 large logs (2.4–5.1 kg); 20–21: shut door	60–74
Cat-Cordwood	50 g paper knots, 0.75 kg kindling; door open	Catalytic combustor bypassed; thermostat knob = 100%	0–1: lighting; 2–4: load 3 small logs (1.4–1.5 kg); 5–6: shut door; 8–9: load 2 large logs (2.2–2.4 kg); 9–10: shut door; 10–11: engage catalytic combustor	60
Pellet	Burn pot clean; hopper filled with Douglas fir pellets	Feed Trim = 4; Combustion Air Trim = 2; Heat Level = 5	0–3: burn-pot fills with pellets; 3–4: 300 W ignitor activates; 4–5: flames established; 10–12: room air fan initiates, automated startup complete	65

Table S4: Low-burn operating protocol for the three heater types. The cordwood heaters begin from a robust bed of hot coals with a fresh fuel load and the door closed; the pellet heater begins from active operation. Each cordwood phase ends when less than 1.0 kg of fuel remains in the firebox. Times in the Events column are minutes from reload (cordwood, cat-cordwood) or from heat-level selection (pellet).

Heater	Initial Fuel Load	Initial Settings	Events (time: action)	Duration (min)
Cordwood	2 large logs (1.2 kg) freshly loaded	Burn Rate Air Control = 1; ACC lever pulled to front; ACC air control timer activated	0–5: choked combustion air ^a	50–72
Cat-Cordwood	3 large logs (2.8–2.9 kg) freshly loaded	Catalytic combustor engaged; thermostat knob = 100%	5: reduce thermostat knob from 100% to 85%; 10: reduce thermostat knob from 85% to 70%	122–163
Pellet	Hopper filled with Douglas fir pellets	Feed Trim = 4; Combustion Air Trim = 2; Heat Level = 2	120–125: heater turned off, pellet burn-out begins	130–135

^a This only occurred for Test 2 and was an operator error.



Figure S2: Images of the cordwood heater high-burn phase paper knots (a), kindling (b), small fuel logs (c), large fuel logs (d), air-control settings (e), firebox before lighting (f), and firebox after all fuel is loaded (g).

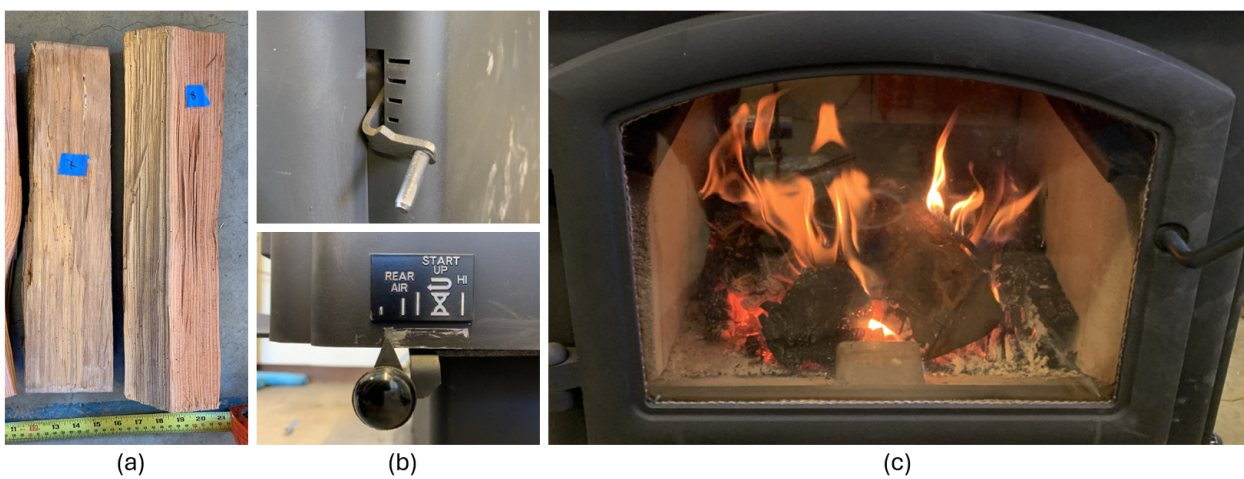


Figure S3: Images of the cordwood heater low-burn phase fuel logs (a), air-control settings (b), and firebox after loading the fuel (c).



Figure S4: Images of the catalytic-cordwood heater high-burn phase paper knots (a), kindling (b), small fuel logs (c), large fuel logs (d), air-control settings (e), firebox before lighting (f), and firebox after all fuel is loaded (g).

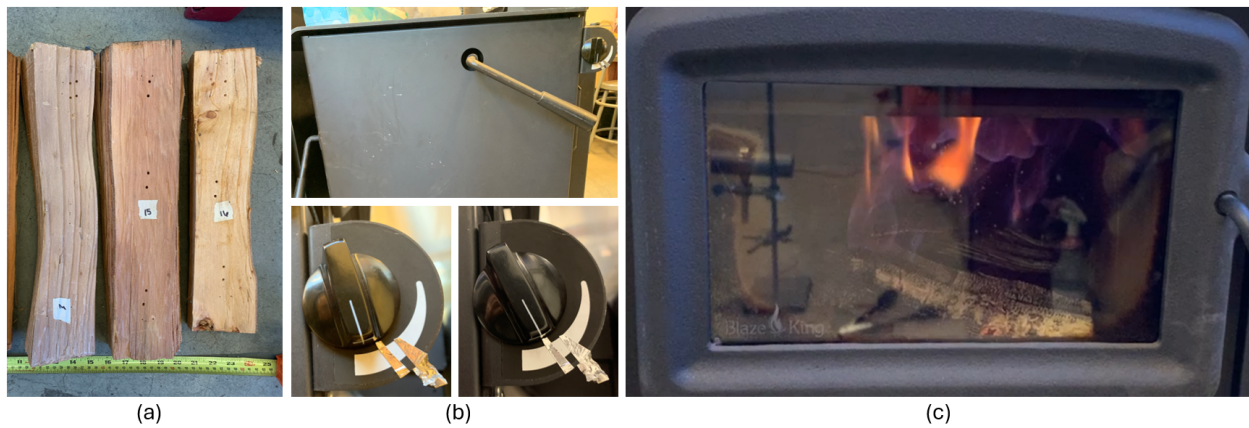


Figure S5: Images of the catalytic-cordwood heater low-burn phase fuel logs (a), air-control settings (b), and firebox after loading the fuel (c).

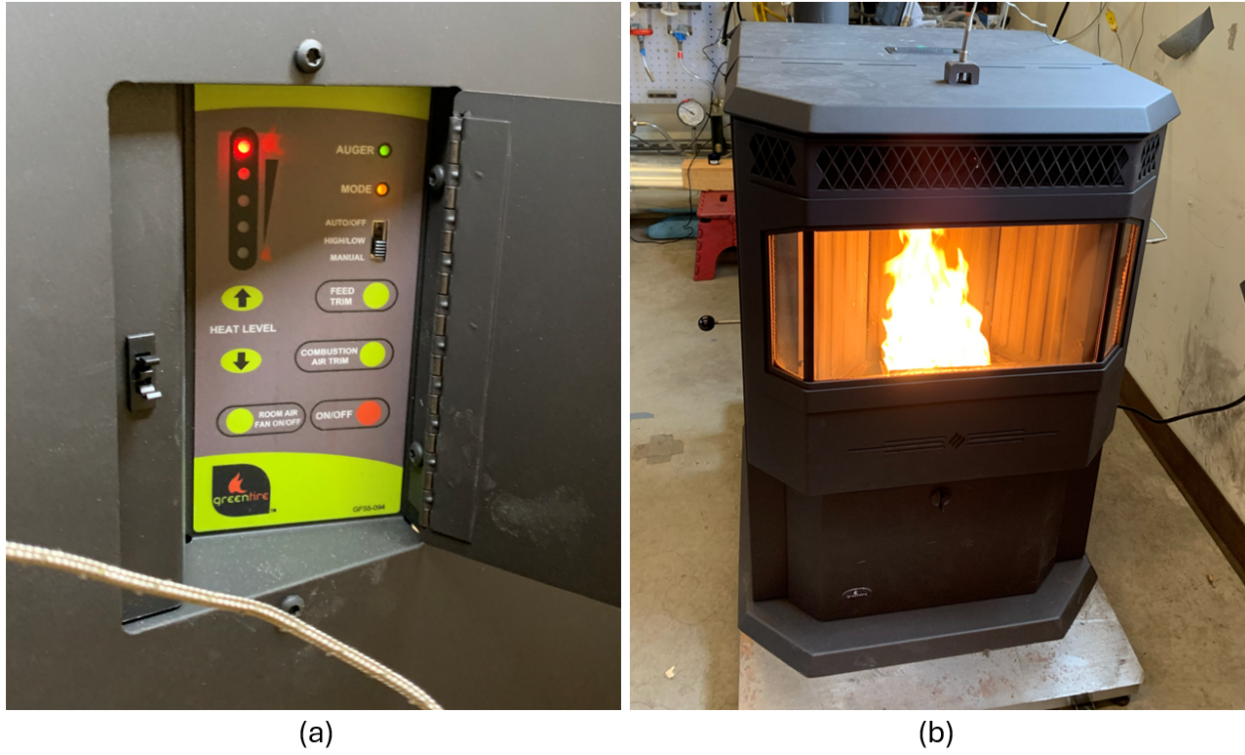


Figure S6: Images of the pellet heater high-burn phase thermostat settings (a), and firebox (b).

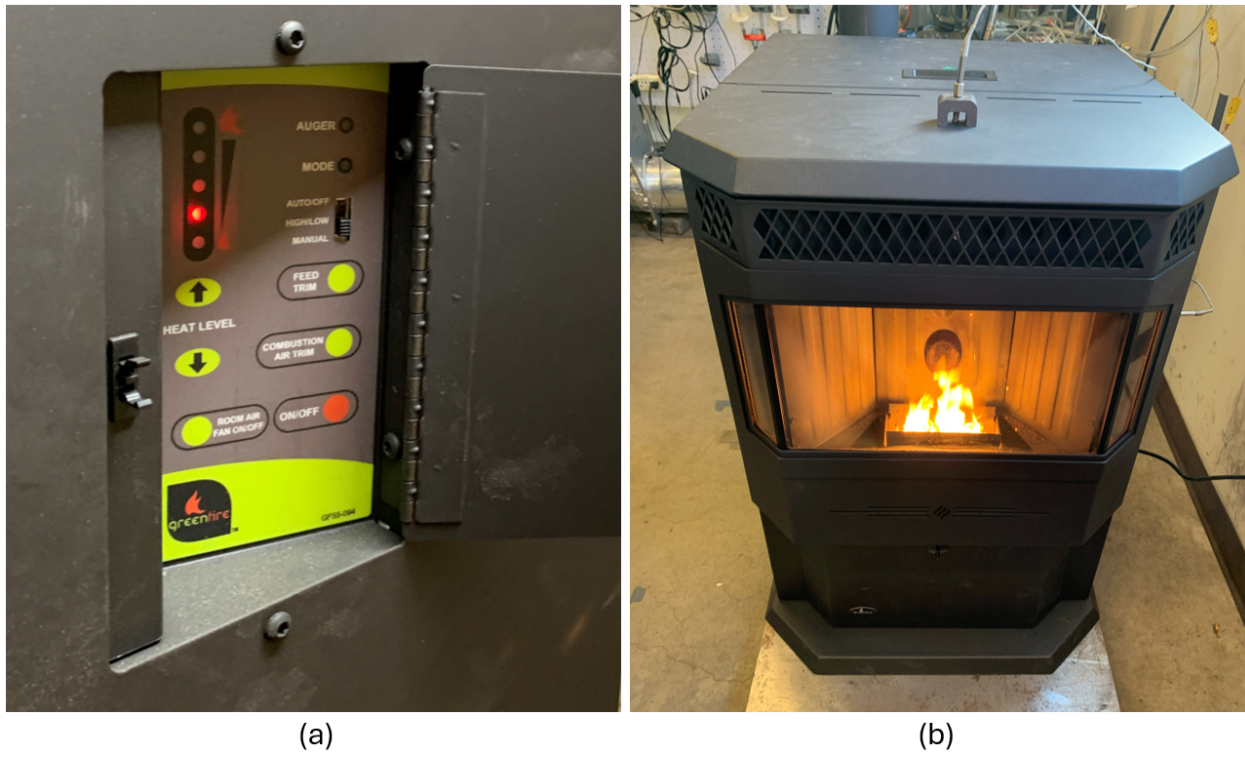


Figure S7: Images of the pellet heater low-burn phase thermostat settings (a), and firebox (b)

S-1.4. Fuel Properties

All heaters were fueled with Douglas Fir seasoned cordwood sourced locally in 2023 or pellets purchased in 2020. Cordwood fuel moisture content (dry-basis) was assessed daily using a pin-type handheld moisture meter with 5/16-inch uninsulated electrodes [21]. Average moisture content of logs used per phase is shown in Table S5. Pellet fuel moisture content was assessed weekly following Method B of the oven-drying procedure described in ASTM D4442 [9]. Fuel charges were weighed on a 10 kg balance (0.1 g readability), and heaters were installed on a 200 kg platform scale (0.05 kg readability, 1 Hz logging) to monitor fuel mass burned throughout each test. Fuel properties, including ultimate analysis and heating values, are reported in Tables S6 and S7.

Table S5: Fuel moisture content (dry basis, %) by heater and phase.

Phase	Test	Catalytic-Cordwood (%)	Cordwood (%)	Pellet (%)
High	1	9.29	9.86	5.89
	2	10.00	9.87	5.89
Low	1	9.92	10.48	5.89
	2	10.19	9.52	5.89

Table S6: Fuel analysis results from Douglas fir cordwood sample.

Moisture, Total D3173 (wt%)	Ash, Total D3174		Heating Value E711		Carbon D5373	H ₂ D5373	N ₂ D5373	O ₂ , Calc.
	As Rec. (wt%)	Moist. Free (wt%)	As Rec. (BTU/lb)	Moist. Free (BTU/lb)	Moist. Free (wt%)	Moist. Free (wt%)	Moist. Free (wt%)	Moist. Free (wt%)
10.15	0.01	0.01	8,187	9,112	49.52	6.3	<0.1	44.1

Table S7: Fuel analysis results from pellet sample.

Parameter	Method	Units	Moisture Free	As Received
Ash	ASTM D1102	wt.%	0.16	0.16
Volatile Matter	ASTM D3175	wt.%	84.12	82.27
Fixed Carbon (by difference)	ASTM D3172	wt.%	15.72	15.38
Sulfur	ASTM D4239	wt.%	0.013	0.012
SO ₂	Calculated	lb/mmbtu	—	0.029
Net Cal. Value (Const. Pressure)	ISO 1928	GJ/tonne	18.48	18.02
Gross Cal. Value (Const. Vol.)	ASTM E711	Btu/lb	8,735	8,543
Carbon	ASTM D5373	wt.%	47.33	46.29
Hydrogen*	ASTM D5373	wt.%	8.51	8.32
Nitrogen*	ASTM D5373	wt.%	<0.20	<0.20
Oxygen*	ASTM D3176	wt.%	>43.79	>42.83

*As-received values do not include hydrogen and oxygen in the total moisture.

S-1.5. Size-resolved Instrument Settings

The size-resolved mass reference was reconstructed from three particle size spectrometers: a TSI 3321 Aerodynamic Particle Sizer (APS), TSI 3330 Optical Particle Sizer (OPS), and TSI 3091 Fast Mobility Particle Sizer (FMPS). Settings for each instrument are as follows:

TSI Model 3091 Fast Mobility Particle Sizer (FMPS). The FMPS was left at default settings, measuring particle count and size distribution at 1 Hz for sizes ranging from 5.6 nm to 560 nm (mobility diameter). Its measurable concentration range varies from 10^2 – 10^7 particles/cc for the smallest particles, to 1 – 10^5 particles/cc for the largest particles. To preserve measurement accuracy, the electrometers were cleaned every 2 test-days.

TSI Model 3330 Optical Particle Sizer (OPS). The OPS was operated with the following user-input settings:

- Particle Density = 1.26
- Refractive index real=1.56, imaginary = 0.03, shape CF=1
- Dead Time Correction enabled

The instrument measures particle count and size distribution at 1 Hz for size ranging from 0.3 μm to 10 μm (optical diameter). It implements a light scattering technique (660 nm wavelength laser; 120 degree light collection) and has a measurable concentration range of 0–3000 particles/cc. Its native 37 mm filter cartridge enables gravimetric sampling that was not used in this study.

TSI Model 3321 Aerodynamic Particle Sizer (APS). The APS was left at default settings, measuring particle count and size distribution at 1 Hz for sizes ranging from 0.5 μm to 20 μm (aerodynamic diameter). It has a measurable concentration range of 0.001 – 10^4 particles/cc.

S-2. Supporting Results

S-2.1. Filter Temperature Comparison

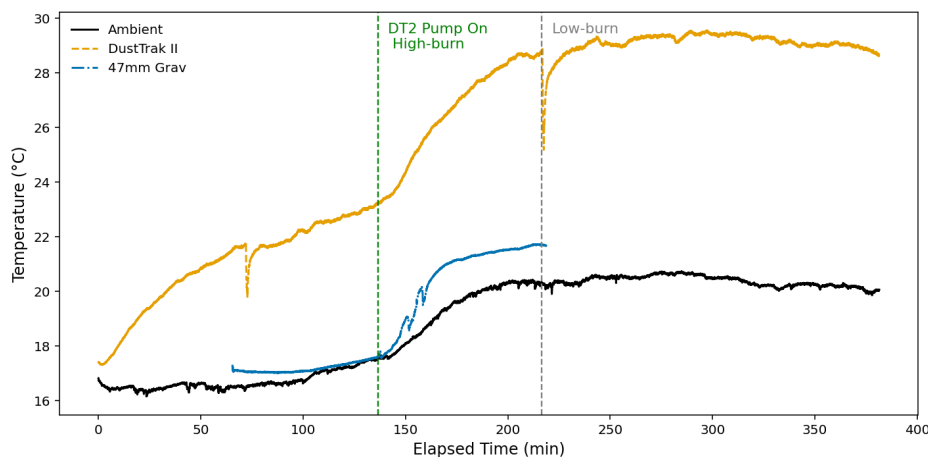


Figure S8: Temperature measurements recorded near the DustTrak II filter cassette, in the reference gravimetric filter holder (47mm Grav), and in the room (Ambient). The dashed vertical line indicates the time at which the heater was ignited, the DustTrak II pump was activated, and flow through the 47mm Grav filter was started. Temperatures near the DustTrak II filter cassette remained elevated above ambient throughout operation and continued to rise over the first hour of pump operation, approaching peak values at approximately the time low-burn sampling phases would typically begin. Ambient and 47mm Grav temperatures also increased following heater ignition as the test space warmed.

S-2.2. Instrument Correction Factors

Table S8: Gravimetric correction factors for each continuous PM instrument, heater type, and operating phase. The correction factor represents the ratio of the gravimetric reference mass to the integrated real-time mass recorded by the instrument over the phase.

Heater	Phase	DT2	pDR	PP8306	TEOM A	TEOM B	Sintrol
Non-Catalytic Cordwood	Startup 1	0.570	3.168	4.716	0.962	1.047	1.711×10^{-1}
	Startup 2	0.393	1.848	2.401	1.115	1.105	1.848×10^{-1}
	High 1	0.454	2.100	2.129	1.087	1.025	2.089×10^{-1}
	High 2	0.634	1.844	2.351	1.736	1.757	8.103×10^{-2}
	Low 1	0.709	1.311	1.585	-15.322	14.851	-3.709×10^{-2}
	Low 2	0.264	15.837	1.974	1.343	1.354	1.810×10^{-1}
Catalytic Cordwood	High 1	0.288	1.033	2.475	-1.043	1.006	6.061×10^{-4}
	High 2	0.367	1.222	2.121	1.149	1.158	3.871×10^{-4}
	Low 1	0.211	0.916	1.021	1.304	-0.064	2.279×10^{-4}
	Low 2	0.270	0.637	0.878	2.034	1.925	2.353×10^{-4}
Pellet	High 1	1.167	5.740	8.741	1.025	1.053	7.055×10^{-2}
	High 2	0.898	4.360	11.413	0.940	0.949	1.513×10^{-1}
	Low 1	3.344	12.714	3.733	1.223	1.245	1.475×10^{-2}
	Low 2	2.801	9.590	5.740	1.821	1.700	-3.841×10^{-3}

S-2.3. Size resolved particle distribution

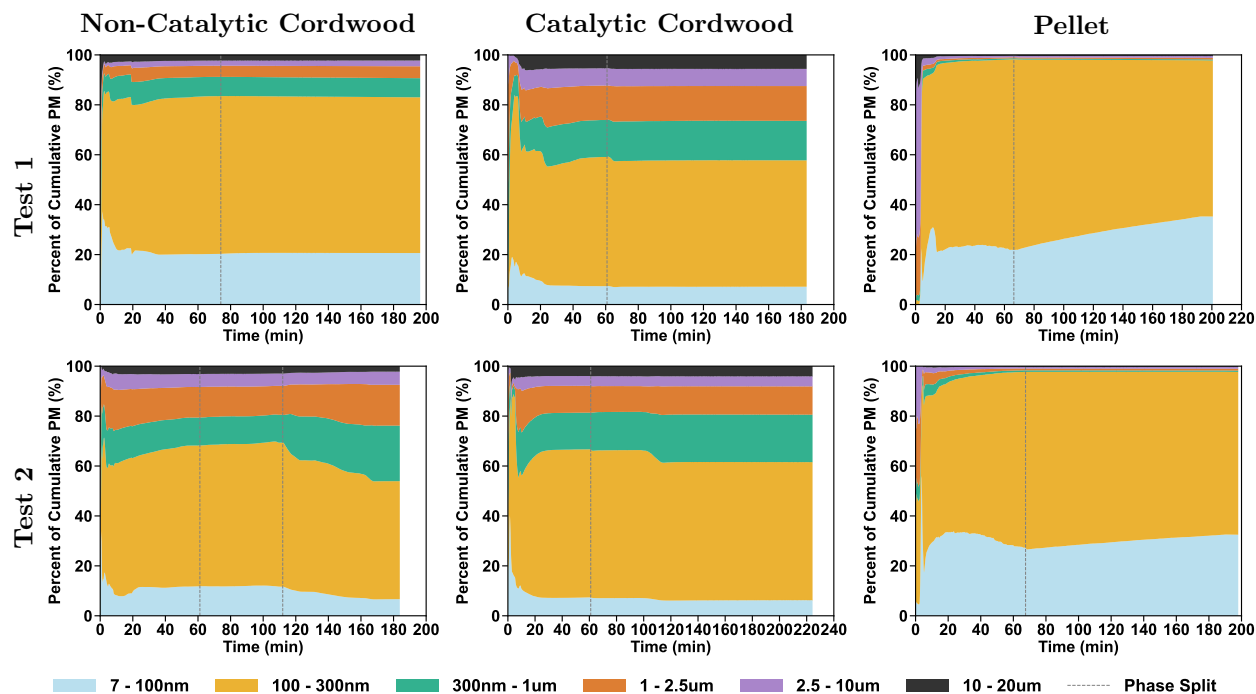


Figure S9: Stacked area plot showing the size distribution of cumulative PM mass as a function of time for the non-catalytic cordwood heater, catalytic cordwood heater, and pellet heater for each test day. The gray vertical lines separate the high-burn and low-burn phases. For the second non-catalytic cordwood test, the high-burn was followed by two low-burns. At each time step, the cumulative mass in each size bin is expressed as a fraction of the total cumulative mass collected up to that point, such that the stack sums to 100% throughout the test.

S-2.4. Calculated average particle densities

Calculated particle densities using measurements from the FMPS, APS, and OPS are shown in Table S9.

Table S9: Fuel density (g/cm^3) for each heater by test phase. Two replicate runs are shown per condition.

Phase	Run	Non-Catalytic Cordwood	Catalytic-Cordwood	Pellet
High	1	1.365	1.308	1.226
	2	1.363	1.301	1.113
Low	1	1.624	1.290	1.374
	2	1.443	1.623	1.201

S-2.5. Cumulative PM Mass

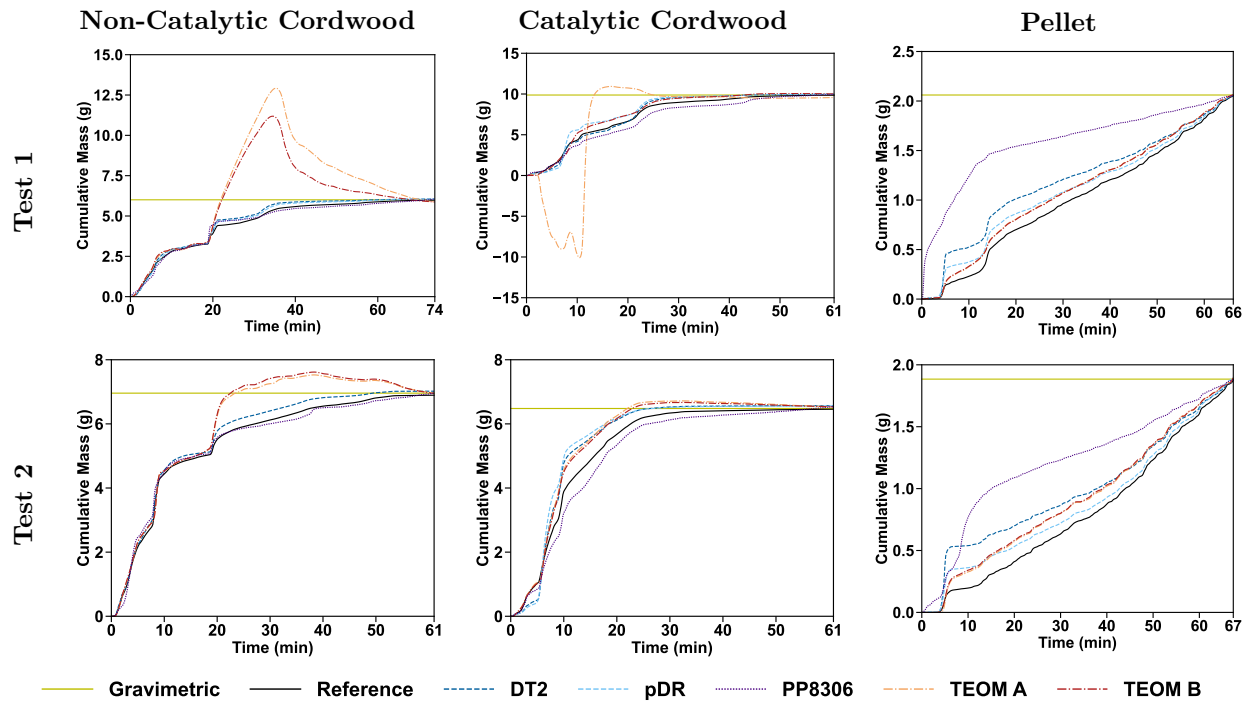


Figure S10: Cumulative PM mass during high-burn phase for three heater types (columns) and two replicate tests (rows). Yellow solid line is the gravimetric measurement reference and the black solid line is the size-resolved mass reference.

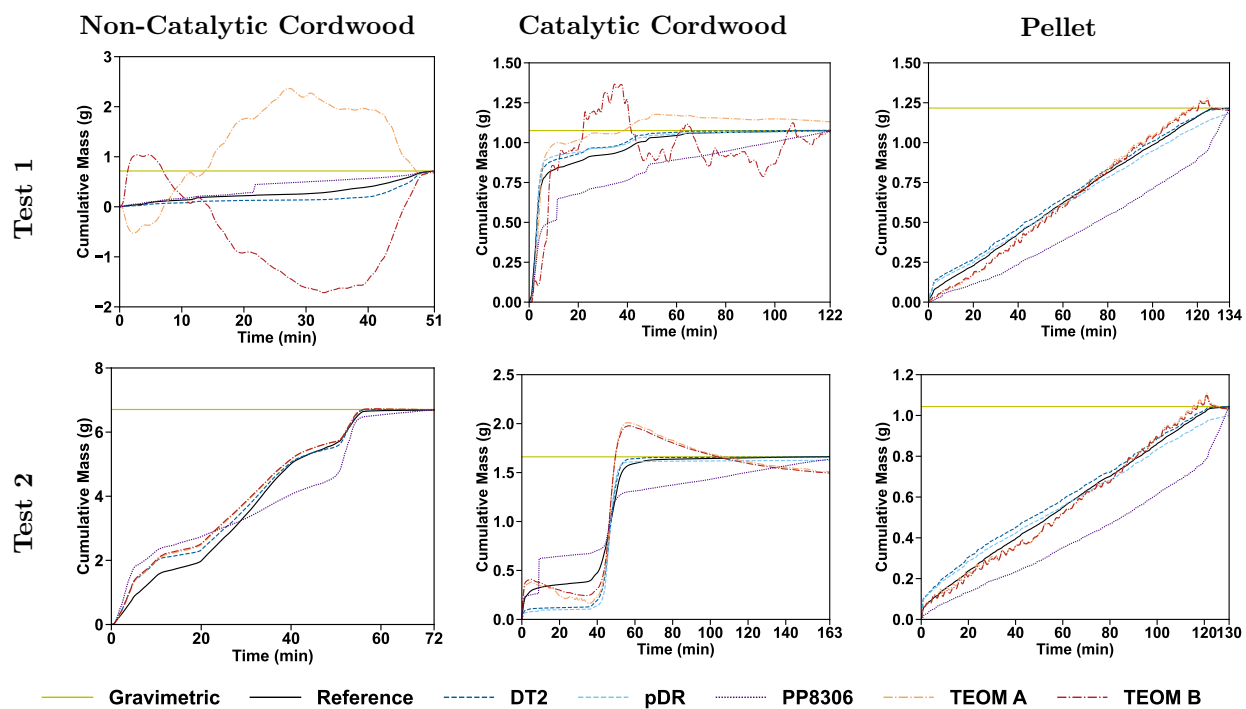


Figure S11: Cumulative PM mass during lo-burn phase for three heater types (columns) and two replicate tests (rows). Yellow solid line is the gravimetric measurement reference and the black solid line is the size-resolved mass reference.

S-2.6. Detailed Description of Particle Instruments Evaluated

Table S10: In depth overview of particulate instruments evaluated.

	DustTrak II 8530	pDR-1500	Particles Plus 8306	1405-D TEOM ^a	Sintrol S203
Operating principle	Optical	Optical	Optical	Mass (TEOM)	Triboelectric
Reports PM0.3	No	No	Calculated	No	No
Reports PM0.5	No	No	Calculated	No	No
Reports PM1	With impactor	With cyclone	Calculated	No	No
Reports PM2.5	With impactor	With cyclone	Calculated	Direct	No
Reports PM4	With impactor	With cyclone	No	No	No
Reports PM5	No	No	Calculated	No	No
Reports PM10	With impactor	With cyclone	Calculated	Direct	No
Reports Total PM	Yes	Yes	Calculated	Yes	No
Native reporting ^a	Total PM	Total PM	PM0.3, PM0.5, PM1, PM2.5, PM5, PM10	PM2.5, PM10, Total PM	TSP
Reports multiple PM bins simultaneously	No	No	Yes; PM0.3, PM0.5, PM1, PM2.5, PM5, PM10	Yes; PM2.5, PM10, Total PM	N/A
Reports PM size distribution	No	No	Yes	No	No
Particle size range	0.1 — 10 µm	0.1 — 10 µm	0.3 — 25 µm (calculated)	None stated — 10 µm	0.3 µm — TSP (200 µm optimal max.)
Particle conc. range ^b	N/A	N/A	530 — 1060 particles/cm ³	N/A	N/A
Conc. range ^c	0.001 — 400 mg/m ³	0.001 — 400 mg/m ³	0.00001 — 20 mg/m ³	0 — 1000 mg/m ³	0.01 — >1000 mg/m ³
Resolution	0.001 mg/m ³	0.001 mg/m ³	None stated	0.0001 mg/m ³	None stated
Integrated pump	Yes	Yes	Yes	No	N/A
Sample flow rate	1.4 — 3.0 L/min	1.0 — 3.5 L/min	2.83 L/min (fixed)	variable	N/A
Recommended flow velocity	N/A	N/A	N/A	N/A	3 — 40 m/s
Secondary Dilution required ^d	No	No	Yes	No	No
Operational temperature range ^e	0 — 50°C	-10 — 50°C	5 — 40°C	2 — 40°C	-40 — 60°C
Operational humidity range	0 — 95%	10 — 95%	20 — 95%	N/A	None stated — 95%

Continued on next page

Table S10 continued from previous page

	DustTrak II 8530	pDR-1500	Particles Plus 8306	1405-D TEOM ^a	Sintrol S203
Accessories	Impactors	Cyclones	N/A	Vacuum pump ^f	N/A
Weight range ^g	1.6–2.5 kg	1.2 kg	1.0 kg	18 kg	1.5 kg
Dimensions	13.5×21.6×22.4 cm	18.1×14.3×8.4 cm	13.0×10.8×31.1 cm	43.2×48.3×75 cm	65.6×16.8×17.5 cm
External power	115 — 240 VAC	100 — 250 VAC	110 — 240 VAC	100 — 240 VAC	100 — 240 VAC
Battery power	Yes	Yes	Yes	No	No
Internal power	Removable Li-ion battery (up to 2)	4 AA alkaline batteries	Removable Li-ion battery	N/A	N/A
Continuous operation battery life	12 hours with 2 batteries 6 hours with 1 battery	> 24 hours @ 1.2 L/min > 6 hours @ 3.5 L/min	> 10 hours	N/A	N/A
Sampling interval range	1 s — 1 hr	1 s — 1 hr	1 s — 99 hr	10 s — 1 hr	None stated
Zero calibration	Yes (user)	Yes (user)	Zero check only	Not available	Zero check only
Average setup time	< 15 min	< 15 min	< 15 min	> 1 hr	< 15 min
Recommended factory calibration interval	1 yr	1 yr	1 yr	1 yr	Application dependent
Gravimetric correction	Required; integrated 37 mm filter	Required; integrated 37 mm filter	Required; external filter	Not required (direct mass)	N/A (TSP only)
Onboard gravimetric measurement	Yes (37 mm)	Yes (37 mm)	No	N/A	No
Cost per test filter replacement	\$2.20	\$2.20	N/A	\$80 (requires two filters)	N/A
Sample downtime after filter change	0 min	0 min	N/A	20 min	N/A
Communication	USB, Ethernet, flash	USB, Ethernet, flash	USB, Ethernet, RS-485, RS-232, Wi-Fi, flash	RPComm software and RS-232, or flash	Analog 4-20 mA and RS-485
Internal storage capacity	60,000 samples	500,000 samples	45,000 samples	500,000 samples	PC log only
Manufacturer support available	Yes	Yes	Yes	No ^h	Yes
Approx. cost (USD) ⁱ	\$8,600	\$10,000	\$5,000	\$25,000–40,000	\$5,000

^a Measurement outputs without any accessories such as impactors or cyclones.

^b Particle concentration range.

^c Aerosol concentration range.

^d Additional dilution required for measurement.

^e Relative humidity, non-condensing.

^f While the impactors and cyclones are optional accessories for the DustTrak and pDR, respectively, the vacuum pump is required for TEOM operation.

^g The DustTrak can be operated with one, two, or zero batteries.

^h Thermo Scientific will discontinue the 1405-D TEOM on June 30, 2026.

ⁱ Estimated 2026 USD.

^j R² calculated from 10-s averaged data with regression through the origin. TEOM R² represents the best performing channel per phase.

^k This range represents the best performing channel for each operational phase.

S-2.7. Parity and Bland–Altman plots

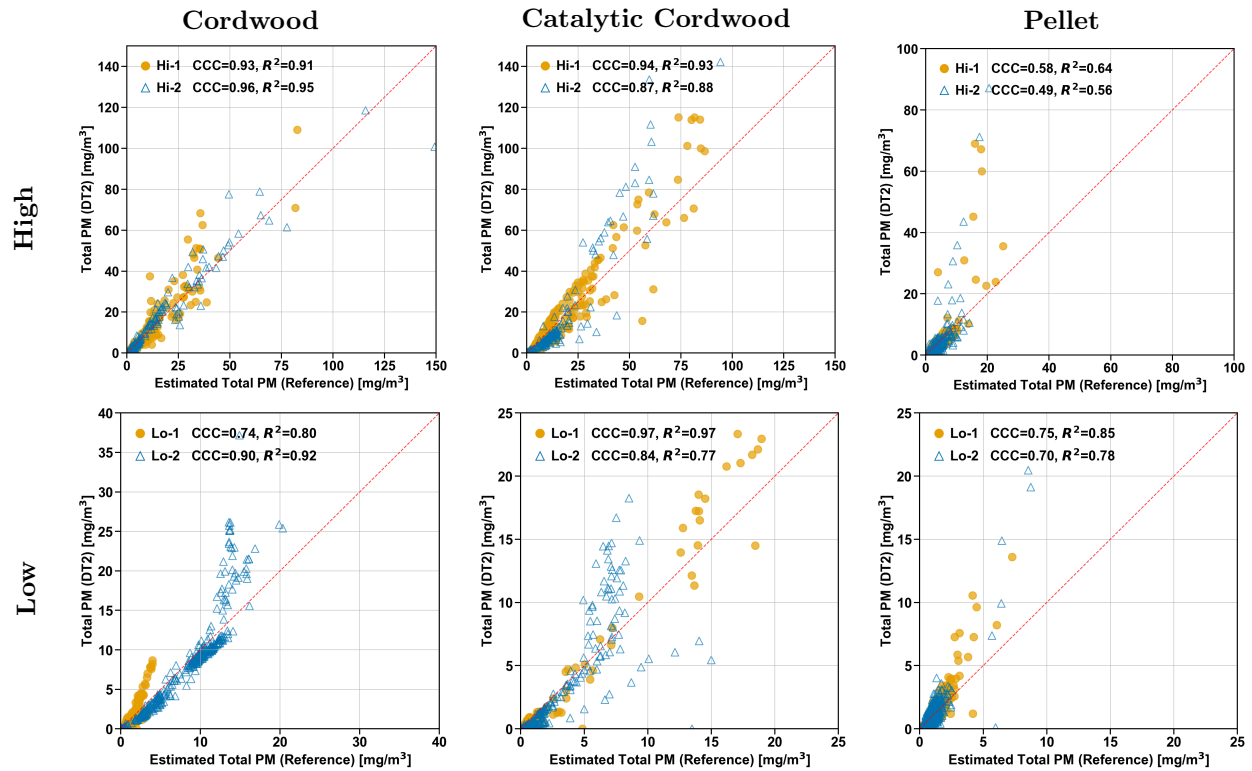


Figure S12: Parity plots of DustTrak II 8530 (DT2) measurements versus the reference total PM mass concentration for three heater types (columns: Cordwood, Catalytic Cordwood, Pellet) and two operating phases (rows: High, Low). Circle and triangle markers denote the two replicate tests within each operating phase, and the red dashed line is the 1:1 reference. Inset values give Lin's concordance correlation coefficient (CCC) [38] and the coefficient of determination (R²) from ordinary least squares regression.

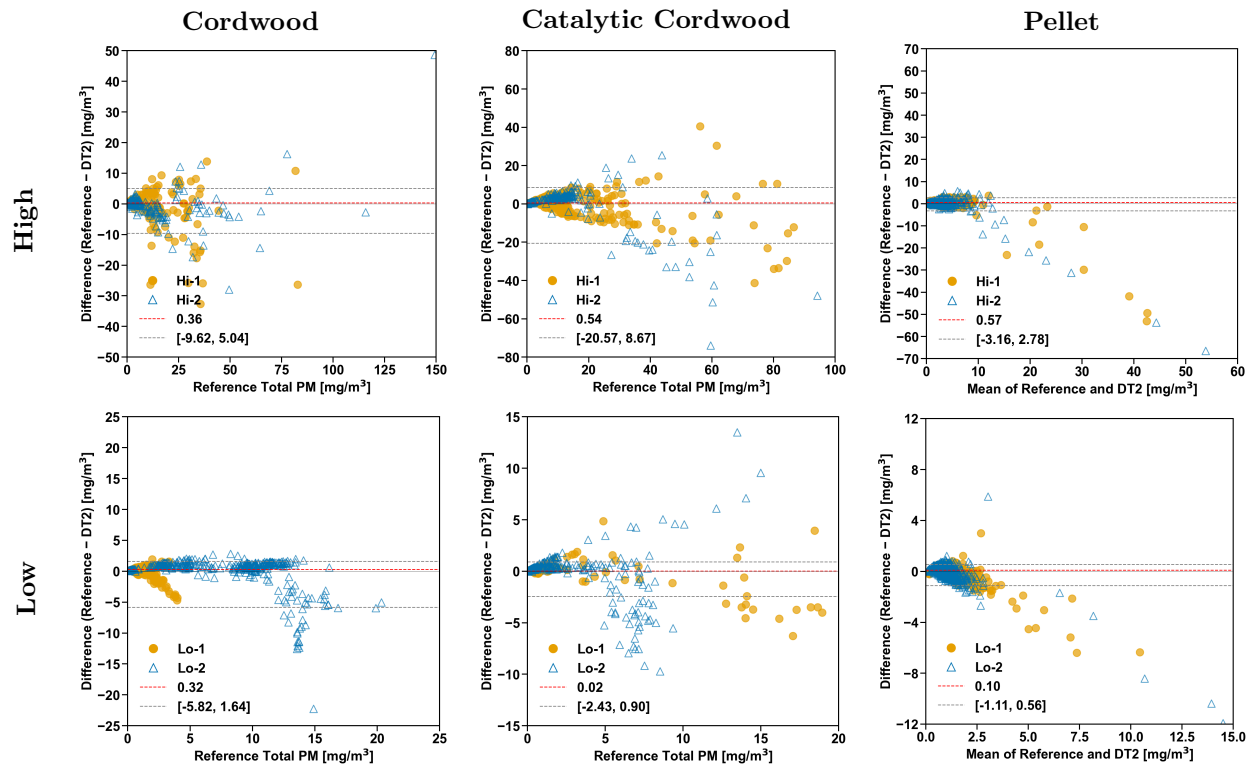


Figure S13: Bland–Altman plots of DustTrak II 8530 (DT2) measurements versus the reference total PM mass concentration for three heater types (columns: Cordwood, Catalytic Cordwood, Pellet) and two operating phases (rows: High, Low). The red dashed line shows the pooled median bias and the gray dashed lines the non-parametric 95% limits of agreement, calculated as the 2.5th and 97.5th percentiles of the pooled differences across both replicates within each panel. The thin black line marks zero difference. Circle and triangle markers denote the two replicate tests within each operating phase as in Figure S12.

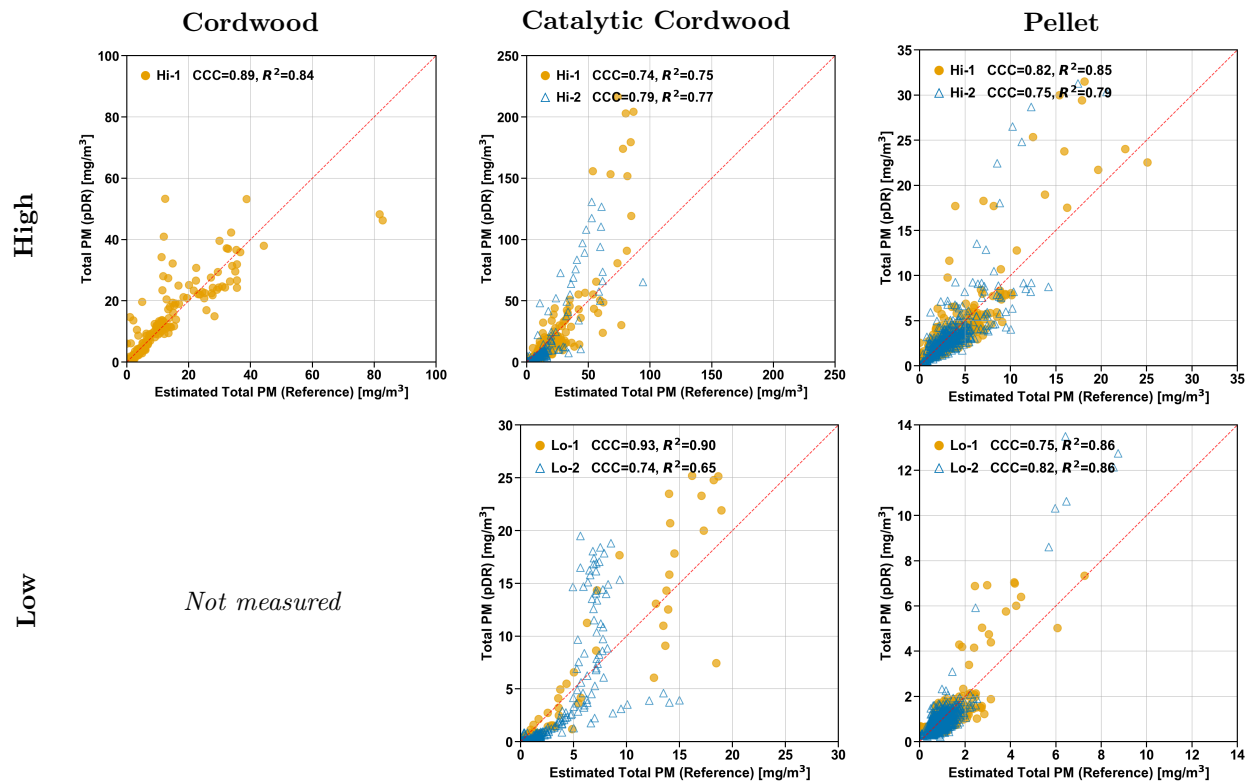


Figure S14: Parity plots of pDR-1500 measurements versus the reference total PM mass concentration for three heater types (columns: Cordwood, Catalytic Cordwood, Pellet) and two operating phases (rows: High, Low). Circle and triangle markers denote the two replicate tests within each operating phase, and the red dashed line is the 1:1 reference. Inset values give Lin's concordance correlation coefficient (CCC) [38] and the coefficient of determination (R²) from ordinary least squares regression.

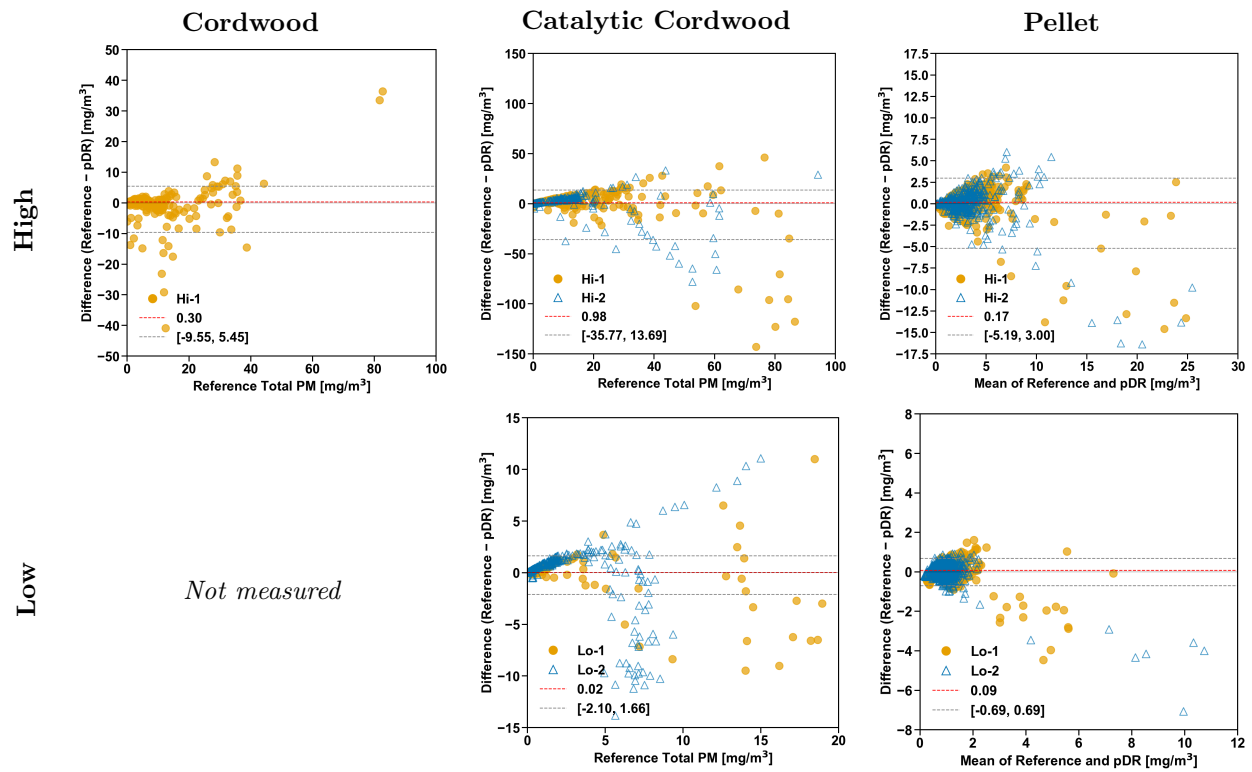


Figure S15: Bland–Altman plots of pDR-1500 measurements versus the reference total PM mass concentration for three heater types (columns: Cordwood, Catalytic Cordwood, Pellet) and two operating phases (rows: High, Low). The red dashed line shows the pooled median bias and the gray dashed lines the non-parametric 95% limits of agreement, calculated as the 2.5th and 97.5th percentiles of the pooled differences across both replicates within each panel. The thin black line marks zero difference. Circle and triangle markers denote the two replicate tests within each operating phase as in Figure S12.

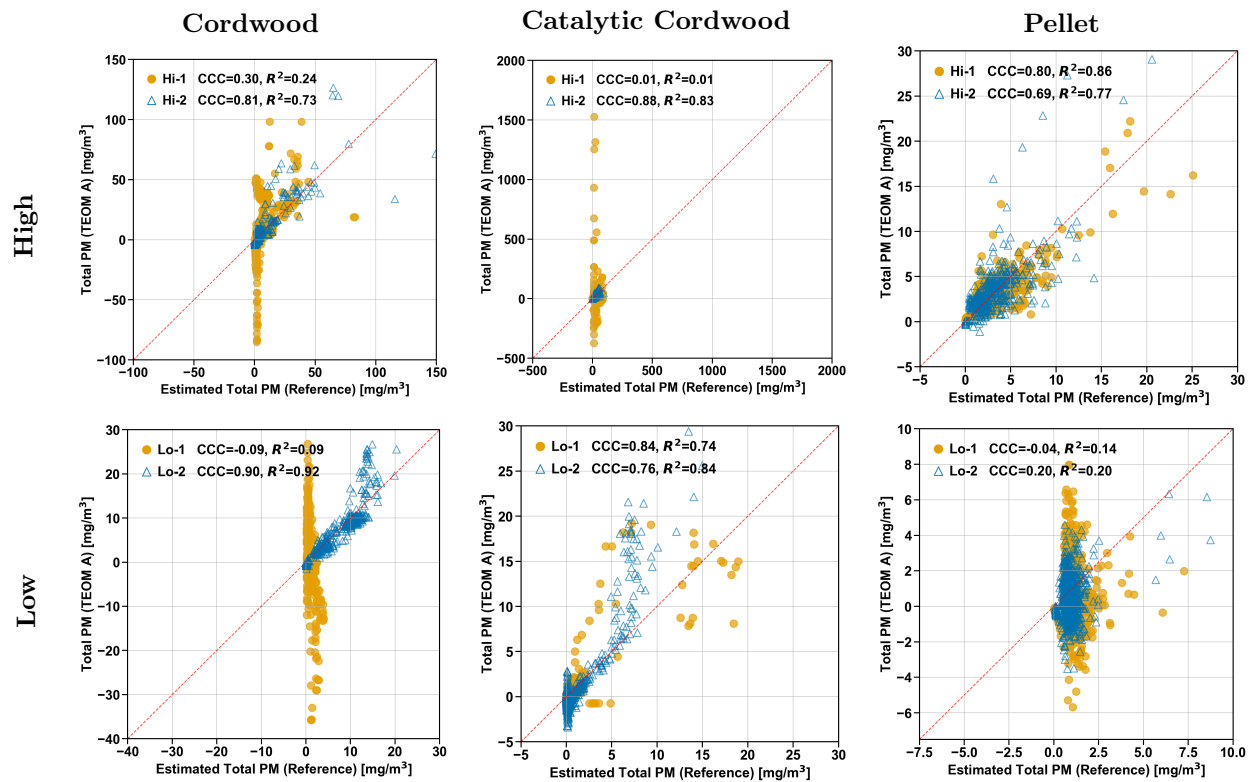


Figure S16: Parity plots of TEOM 1405D Channel A measurements versus the reference total PM mass concentration for three heater types (columns: Cordwood, Catalytic Cordwood, Pellet) and two operating phases (rows: High, Low). Circle and triangle markers denote the two replicate tests within each operating phase, and the red dashed line is the 1:1 reference. Inset values give Lin's concordance correlation coefficient (CCC) [38] and the coefficient of determination (R^2) from ordinary least squares regression.

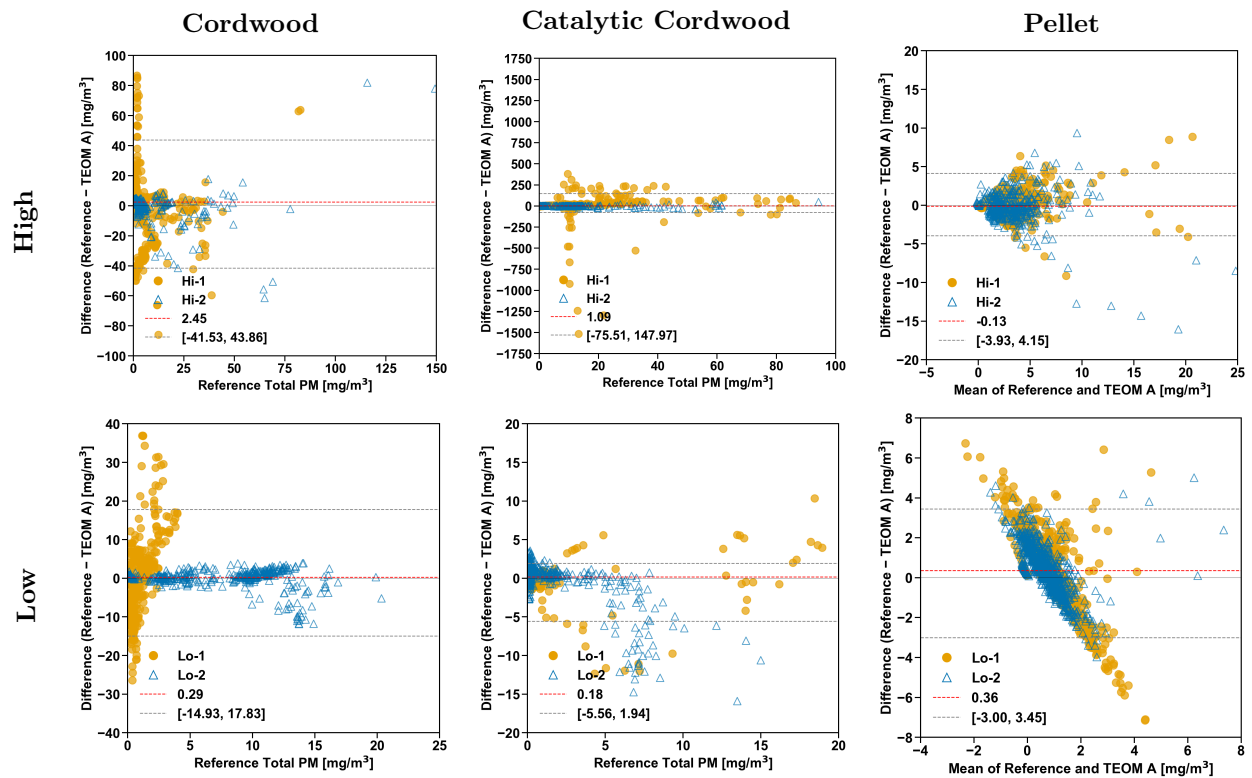


Figure S17: Bland–Altman plots of TEOM 1405D Channel A measurements versus the reference total PM mass concentration for three heater types (columns: Cordwood, Catalytic Cordwood, Pellet) and two operating phases (rows: High, Low). The red dashed line shows the pooled median bias and the gray dashed lines the non-parametric 95% limits of agreement, calculated as the 2.5th and 97.5th percentiles of the pooled differences across both replicates within each panel. The thin black line marks zero difference. Circle and triangle markers denote the two replicate tests within each operating phase as in Figure S12.

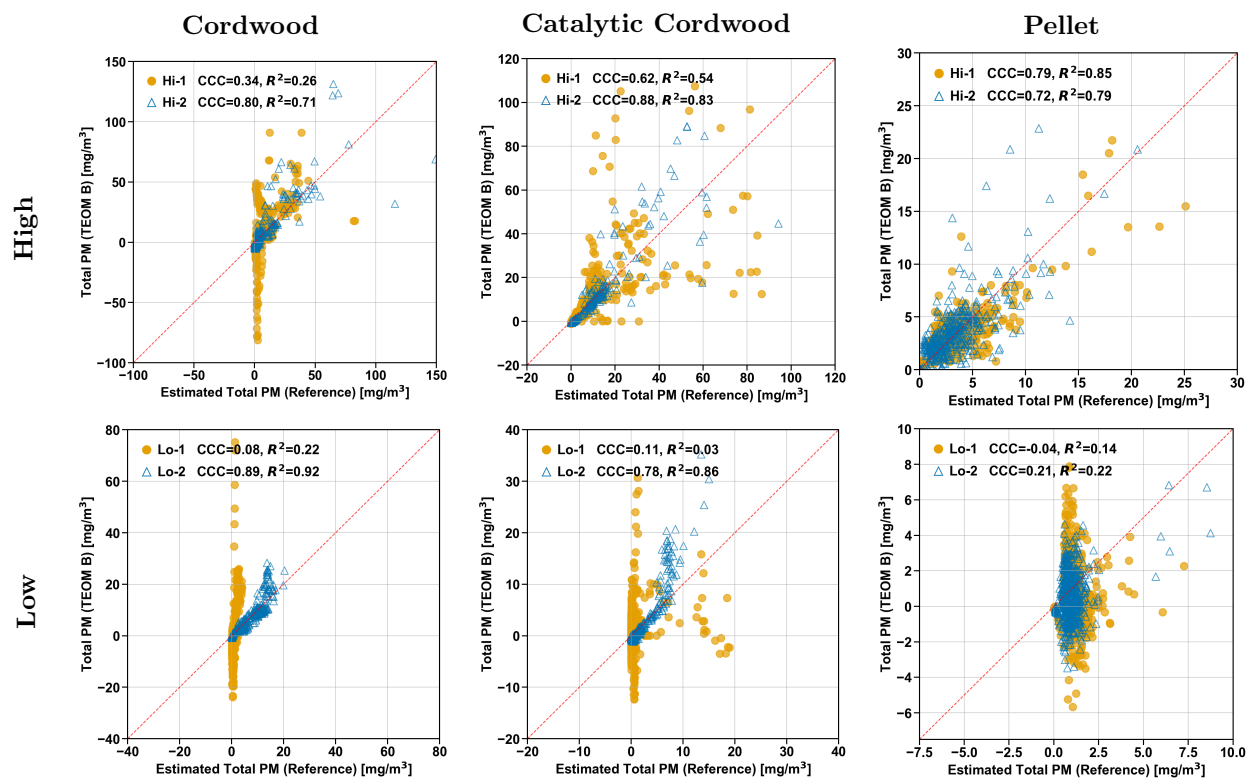


Figure S18: Parity plots of TEOM 1405D Channel B measurements versus the reference total PM mass concentration for three heater types (columns: Cordwood, Catalytic Cordwood, Pellet) and two operating phases (rows: High, Low). Circle and triangle markers denote the two replicate tests within each operating phase, and the red dashed line is the 1:1 reference. Inset values give Lin's concordance correlation coefficient (CCC) [38] and the coefficient of determination (R^2) from ordinary least squares regression.

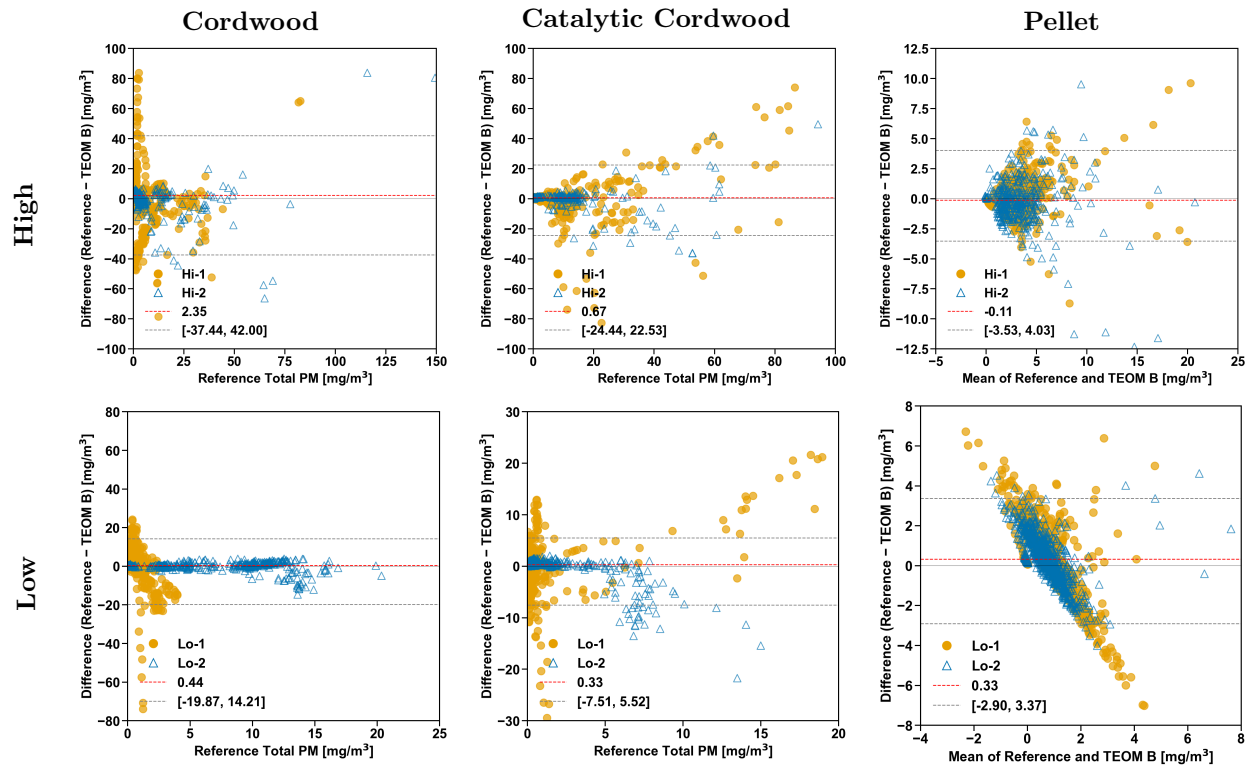


Figure S19: Bland–Altman plots of TEOM 1405D Channel B measurements versus the reference total PM mass concentration for three heater types (columns: Cordwood, Catalytic Cordwood, Pellet) and two operating phases (rows: High, Low). The red dashed line shows the pooled median bias and the gray dashed lines the non-parametric 95% limits of agreement, calculated as the 2.5th and 97.5th percentiles of the pooled differences across both replicates within each panel. The thin black line marks zero difference. Circle and triangle markers denote the two replicate tests within each operating phase as in Figure S12.

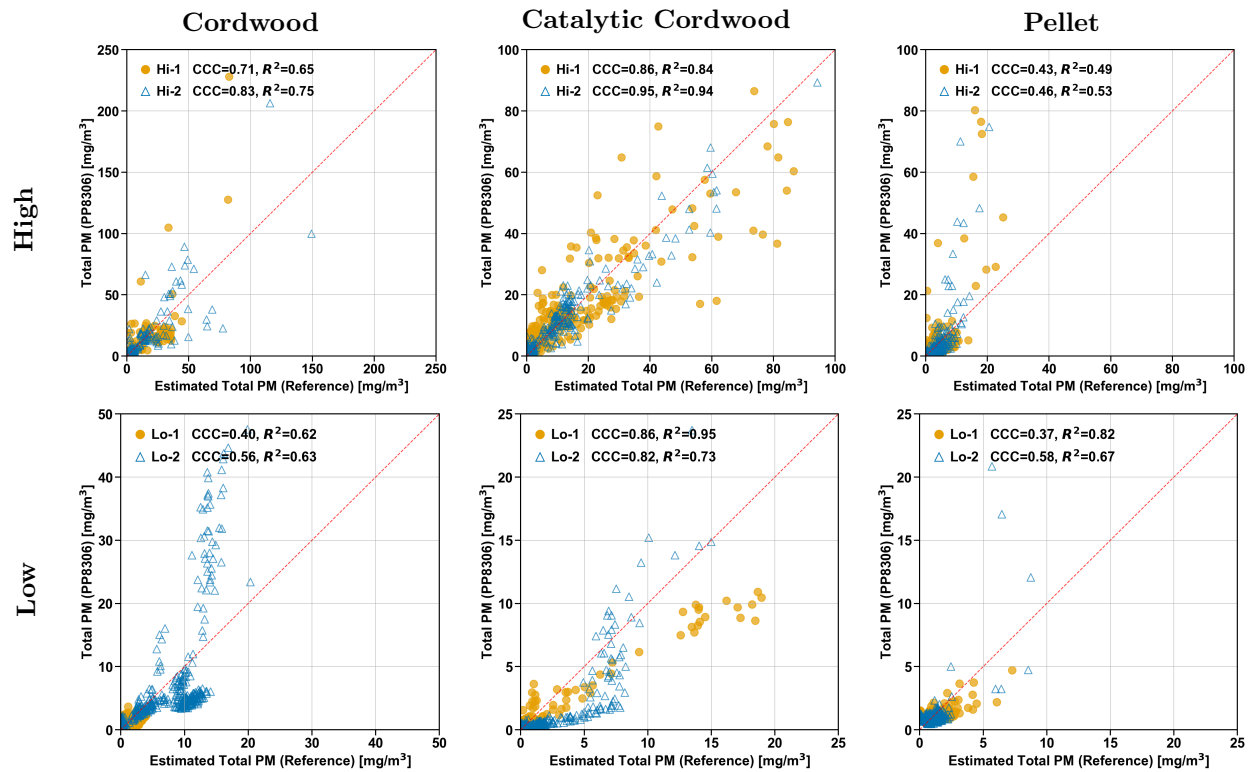


Figure S20: Parity plots of PP8306 measurements versus the reference total PM mass concentration for three heater types (columns: Cordwood, Catalytic Cordwood, Pellet) and two operating phases (rows: High, Low). Circle and triangle markers denote the two replicate tests within each operating phase, and the red dashed line is the 1:1 reference. Inset values give Lin's concordance correlation coefficient (CCC) [38] and the coefficient of determination (R^2) from ordinary least squares regression.

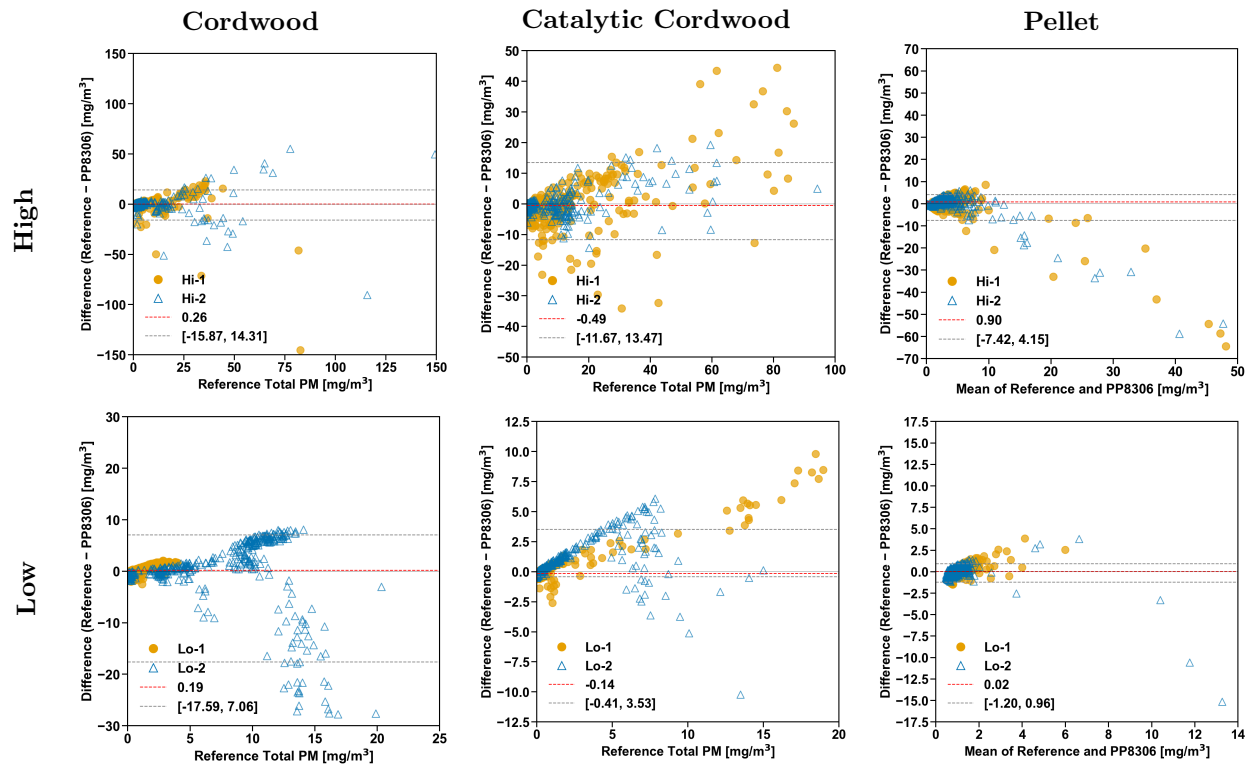


Figure S21: Bland–Altman plots of PP8306 measurements versus the reference total PM mass concentration for three heater types (columns: Cordwood, Catalytic Cordwood, Pellet) and two operating phases (rows: High, Low). The red dashed line shows the pooled median bias and the gray dashed lines the non-parametric 95% limits of agreement, calculated as the 2.5th and 97.5th percentiles of the pooled differences across both replicates within each panel. The thin black line marks zero difference. Circle and triangle markers denote the two replicate tests within each operating phase as in Figure S12.

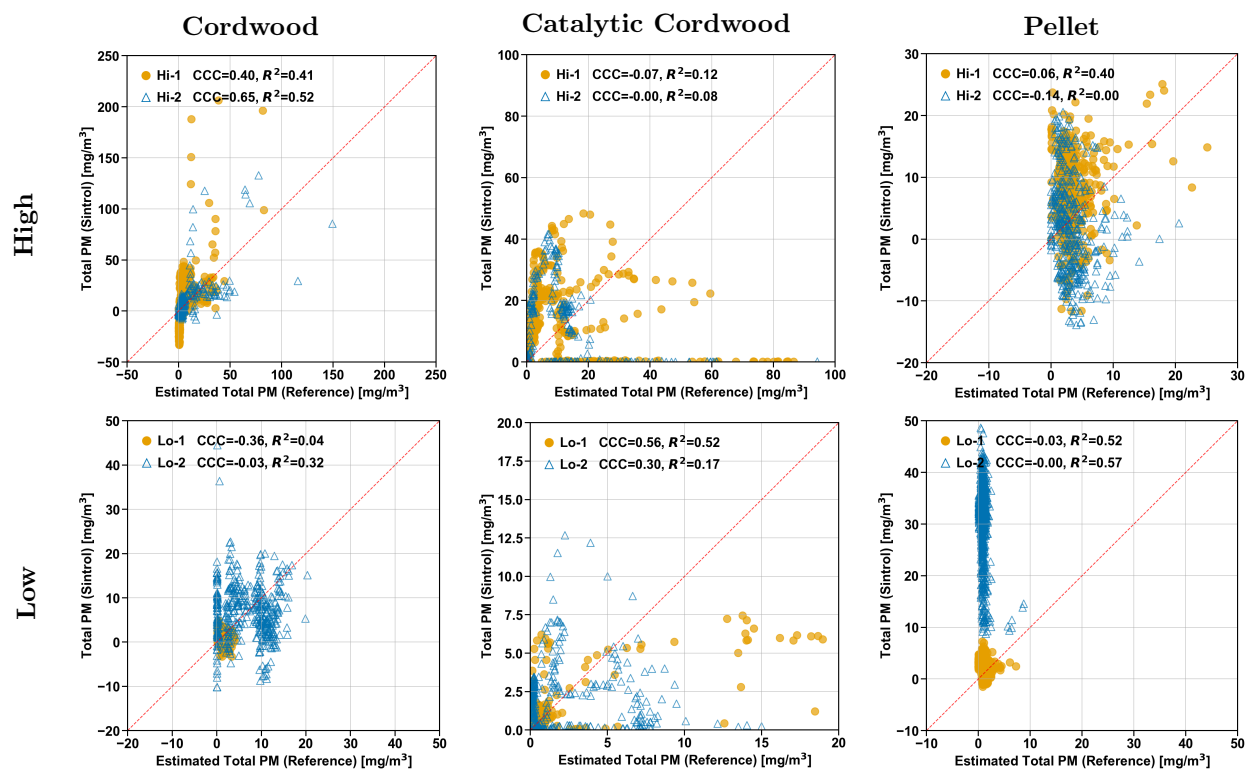


Figure S22: Parity plots of Sintrol S203 measurements versus the reference total PM mass concentration for three heater types (columns: Cordwood, Catalytic Cordwood, Pellet) and two operating phases (rows: High, Low). Circle and triangle markers denote the two replicate tests within each operating phase, and the red dashed line is the 1:1 reference. Inset values give Lin's concordance correlation coefficient (CCC) [38] and the coefficient of determination (R^2) from ordinary least squares regression.

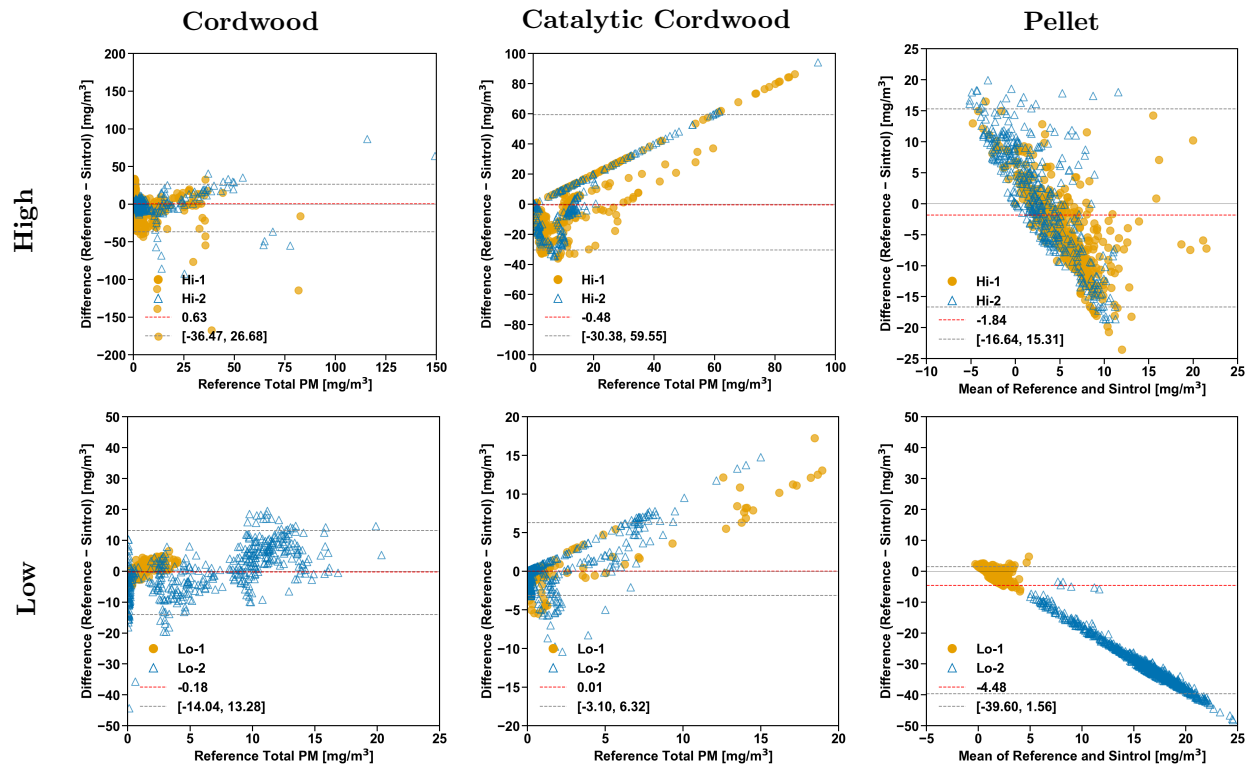


Figure S23: Bland-Altman plots of Sintrol S203 measurements versus the reference total PM mass concentration for three heater types (columns: Cordwood, Catalytic Cordwood, Pellet) and two operating phases (rows: High, Low). The red dashed line shows the pooled median bias and the gray dashed lines the non-parametric 95% limits of agreement, calculated as the 2.5th and 97.5th percentiles of the pooled differences across both replicates within each panel. The thin black line marks zero difference. Circle and triangle markers denote the two replicate tests within each operating phase as in Figure S12.